Modeling and performance enhancement of thermo-active foundations for cold climates - Case of Minnesota

A THESIS
SUBMITTED TO THE FACULTY OF THE
UNIVERSITY OF MINNESOTA DULUTH
BY:

Prem Agarwala

IN PARTIAL FULFILLMENT OF THE REQUIREMENTS
FOR THE DEGREE OF
MASTER OF SCIENCE
IN MECHANICAL ENGINEERING

Dr. Alison Hoxie, Dr. Aggrey Mwesigye

Adviser, Co-adviser

July 2023

Acknowledgments

Dedication

This thesis is dedicated to my parents Pushpa Agarwala and Pradip Kumar Agarwala.

Abstract

In the United States, building energy consumption accounts for approximately 40%, with a significant portion used to meet heating and cooling needs. The reliance on fossil fuels to meet space heating and hot water needs leads to substantial CO_2 emissions. Therefore, there is an urgent need for clean and sustainable energy technologies to decarbonize building energy usage. Among these technologies, ground source heat pump (GSHP) systems have gained significant attention due to their high efficiency and consistent performance across different seasons. However, their widespread adoption is hindered by the high initial costs, despite their lower operation and maintenance expenses. One promising approach to mitigate this issue is coupling the GSHP system's ground heat exchanger with the building foundation, known as the "thermo-active foundation (TAF)." By doing so, the capital cost and space requirements of the entire system can be reduced. Additionally, integrating the ground heat exchanger with the building foundation serves dual purposes of structural support and heat exchange with the ground.

This study focuses on evaluating and enhancing the performance of a vertical U-loop ground heat exchanger integrated into a 20-meter deep helical steel pile. A thoroughly validated and verified transient computational fluid dynamics numerical model is employed for this purpose. The model is utilized to investigate the short-term (one year) and long-term (five years) transient performance of the system in the cold climate of Minnesota, where there is a significant disparity between heating and cooling loads. A building energy model, representing a typical small residential house in Minnesota with an area of 2026 square feet, is developed using BEopt software to determine the annual heating and cooling loads. Three normalized building load cases (0.25, 0.33, and 0.4 tons) are then used to determine the capacity per pile. For the larger 0.4 tons load, detailed parametric studies are conducted to establish performance under different inlet fluid velocities (considering laminar and turbulent flow regimes), and the TAF's location in relation to the building. The results demonstrate that the COP (coefficient of performance) remains constant at around 3.3 for all pile locations, indicating that the system's performance is independent of the pile's location. Moreover, for all flow velocities, the

COP remains the same, around 3.3, with laminar flow being preferable due to lower pump power requirements.

To enhance performance, thermal energy storage using phase change material (PCM), is incorporated inside the TAF. Two PCM tubes, each with a volume of 0.0053093 m^3 (5.30 kg), are inserted beside both sides of the pile in the ground. The performance enhancement for different building loads (0.4 tons, 0.33 tons, and 0.25 tons) is compared to determine the optimal amount of heating load per pile necessary to meet the total building load over a year in Duluth, MN using PCM. The results indicate that a 0.4 tons load per pile is the most economical option, requiring eight piles to meet the house's load in Duluth, MN, with an additional heating requirement during 6.30% of the year. The system's performance is also assessed in other locations in Minnesota, including International Falls and Saint Paul, to compare long-term performance with Duluth for a 0.4 tons building load. The average annual COP using PCM in Duluth, International Falls, and Saint Paul is found to be 4.09, 4.20, and 4.60, respectively, with Saint Paul exhibiting the best performance due to its higher cooling energy demand and low peak heating loads. However, despite having a higher COP than Duluth, International Falls shows the worst performance owing to the high heating loads, thus requiring more auxiliary heating.

Table of Contents

Contributions

1. **Prem Agarwala,** Shayan Davani, Amirhossein Darbandi, Jordan Gruenes, Alison Hoxie, Aggrey Mwesigye, "Thermal Performance Analysis of Helical Steel Thermo-Active Foundations for Cold Climates," In Conference Proceedings of the ASHRAE and SCANVAC HVAC Cold Climate Conference, March 6-8, 2023, Anchorage, Alaska.

2. Shayan Davani, Amirhossein Darbandi, **Prem Agarwala,** Jordan Gruenes, Alison Hoxie, Aggrey Mwesigye, "Design and Performance Analysis of Slinky Type Foundation Heat Exchangers for Space Heating and Cooling in Cold Climate," In Conference Proceedings of the 8th Thermal and Fluids Engineering Conference 2023, ASTFE.

3. Amirhossein Darbandi, Shayan Davani, Jordan Gruenes, **Prem Agarwala,** Alison Hoxie, Aggrey Mwesigye, "Long-Term Thermal Performance Analysis of a Horizontal Foundation Heat Exchanger for Space Heating and Cooling in Extremely Cold Climates," In Conference Proceedings of the 8th Thermal and Fluids Engineering Conference 2023, ASTFE.

4. **Prem Agarwala,** Shayan Davani, Amirhossein Darbandi, Jordan Gruenes, Alison Hoxie, Aggrey Mwesigye, "CFD Study of Vertical U-Loop Thermo-Active Foundations for Cold Climates," In Conference Proceedings of the 75th Annual Meeting, APS DFD 2022, November 20-22, 2022, Indianapolis, Indiana.

List of Tables

List of Figures

Nomenclature

Abbreviations and Acronyms

UNEP	:	United Nations Environment Program
GSHP	:	Ground Source Heat Pump
TAF	:	Thermo-active Foundation
COP	:	Coefficient of Performance
TES	:	Thermal Energy Storage
PCM	:	Phase Change Material
HCF	:	Heat Carrier Fluid
ASHP	:	Air-Source Heat Pumps
GHE	:	Ground Heat Exchanger
BHE	:	Borehole Heat Exchanger
PHC	:	Pre-Stressed High-strength Concrete
HSP	:	Helical Steel Pile
PVC	:	Polyvinyl Chloride
PE	:	Polyethylene
LTHS	:	Latent Heat Storage
MPCM	:	Microencapsulated Phase Change Material

List of Symbols

ρ	:	Density, kg/m^3
$C_{p,s}$	:	Specific heat capacity of the solid, J/kg.K
k_s	:	Thermal conductivity of the solid, W/m.K
P	:	Pressure, Pa
σ_k	:	Turbulent Prandtl numbers for k, Unitless
σ_ε	:	Turbulent Prandtl numbers for ε, Unitless
μ_t	:	Turbulent/eddy viscosity, m^2/s
H	:	Enthalpy of the material, J/kg
h	:	Sensible enthalpy, J/kg
ΔH	:	Latent heat, J/kg
$T_{solidus}$	:	Temperature of the PCM is solid phase, K
$T_{liquidus}$	:	Temperature of the PCM in liquid phase, K
L	:	Latent heat of PCM, J/kg
β	:	Liquid volume fraction, Unitless
A_{mush}	:	Mushy zone constant, $Kg/s.m^3$
V_f	:	Volumetric flow rate, m^3/s

Chapter 1 - Introduction

1.1 Background

Climate change is currently the most alarming global issue across the world. Among various influential factors, burning fossil fuels stands out as one of the most powerful contributors to increase greenhouse gas emissions in the atmosphere. It is widely recognized that the rising emissions of greenhouse gases, including carbon dioxide, will significantly impact global temperature [1]. We must address this concern urgently and take proactive initiatives to reduce environmental carbon emissions. Many developed countries are already taking necessary steps to mitigate this problem. Recently, the United States has passed legislation to reduce greenhouse gas emissions by 1 billion metric tons by 2023 and going net-zero emissions by 2050. The private sector in the U.S. will launch 950 million solar panels, 120,000 wind turbines, and 2300 grid-scale battery plants by 2030 [2]. According to the United Nations Environment Program (UNEP), in 2015, the building sector accounted for 30% of global final energy consumption, with residential buildings contributing 22% and nonresidential buildings contributing 8%. Additionally, energy-related CO_2 emissions from buildings globally amounted to 28%, with residential buildings responsible for 17% and nonresidential buildings contributing 11% [3]. In 2021, the usage of fossil fuels in buildings resulted in approximately 8% of global energy-related and process-related CO_2 emissions [4].

In developed countries, buildings are responsible for around 20-40% of carbon emissions [5]. In the United States, building energy consumption accounts for roughly 40%, with a significant portion dedicated to meeting heating and cooling demands [6]. Common heating and cooling systems include natural gas, electric resistance heating, and central air-conditioning. The fuel consumption associated with operating these systems leads to substantial CO_2 emissions being released into the environment.

Ground source heat pumps (GSHPs) or geothermal heat pumps are highly efficient renewable energy technologies used for space heating and cooling purposes, offering the potential to decarbonize building energy use, especially when powered by renewable

electricity. GSHPs utilize the ground as a heat source during winter and a heat sink during summer, reducing the building's electricity demand for heating and cooling. The stable ground temperature at lower depths throughout the year allows the system to efficiently meet buildings' heating and cooling energy needs. The electrical energy required for the building's air conditioning comes down to only the amount needed to operate the heat pump [7]. Moreover, GSHPs are 65% more energy-efficient than traditional HVAC systems, making them an ideal choice for implementing heating and cooling systems in buildings [8].

1.2 Problem Statement

Generally, balanced GSHPs undergo a natural thermal recovery or recharging process, where the heat extracted during winter is restored in summer, and vice versa [9]. For GSHP systems, the ground temperature is relatively stable compared to ambient air temperatures, ensuring the stable performance of the GSHP systems. Despite their great potential for reducing carbon emissions, the use of GSHPs is hindered by their high capital cost and land area requirements [10]. To address this issue, GSHPs coupled with building foundations, known as "Thermo-active Foundation (TAF)," have recently gained popularity.

The heat exchangers in TAF are realized by inserting pipes containing a heat transfer fluid into the building foundation piles. These piles serve a dual purpose by providing structural support and facilitating heat exchange with the ground through the flowing heat transfer fluid in the heat exchanger with the help of a GSHP coupled to the system.

While numerous studies have focused on TAF, limited research has been conducted on the performance of these systems in extremely cold conditions, where the heating load surpasses the cooling load throughout the year. Additionally, the effect of energy pile location on long-term system performance remains unexplored.

Moreover, in extremely hot or cold climates, thermal imbalance in the ground temperature can occur due to uneven building energy loads. Prolonged heat extraction during the heating season to warm the building gradually lowers the ground temperature, resulting in

2

reduced system efficiency. A similar process occurs during the cooling season for long-term cooling demand. Consequently, the optimal performance of GSHPs may be compromised, leading to a lower coefficient of performance (COP) and long-term system failure [11]. To mitigate these thermal imbalance issues caused by unbalanced heating or cooling loads, additional thermal energy storage (TES) systems should be integrated into heating-dominated and cooling-dominated climate conditions [12]. Energy storage systems play a vital role in effectively utilizing renewable energy and conserving energy. They can harness stored heat or cold that would otherwise go to waste [13]. Therefore, integrating TES systems with GSHP systems, particularly by utilizing phase change materials (PCM), offers a promising solution to address the thermal imbalance problems associated with unbalanced heating or cooling loads [12].

However, limited research is available integrating GSHPs with PCM for actual building loads, especially in cold climates. Additionally, the impact of PCM on the performance of building heating and cooling systems, as well as the performance of GSHPs, requires further investigation for both short-term and long-term operations.

1.3 Objectives

The specific objectives of this research are:

1. Evaluate the long-term performance of helical steel thermo-active foundation (TAF) in different locations within the state of Minnesota to represent cold climate conditions. The representative locations are Duluth, International Falls, and Saint Paul.

2. Assess the system's performance under actual building loads for both short-term (one year) and long-term (five years) scenarios, considering various inlet velocities.

3. Investigate the impact of different pile locations, including those near the ground surface and beneath the building foundation, on the performance of TAF systems.

4. Evaluate the potential improvements in performance with the integration of Phase Change Material (PCM) in the TAF system and actual building loads, considering both short-term and long-term operations.

1.4 Organization of the Thesis

This thesis is organized into five chapters. Chapter 1 presents the introduction, background, and objectives of the thesis. Chapter 2 presents an updated literature review. Chapter 3 shows the numerical modeling procedure. Chapter 4 shows the results of the parametric studies together with the validation and verification of the developed numerical model. Chapter 5 shows the enhancements of TAFs for different locations in Minnesota. Chapter 6 presents the conclusion of the thesis. Chapter 7 gives recommendations for future studies, and the references are enlisted used in this study at the end.

Chapter 2 - Literature Review

2.1 Introduction and Operating Principle of a GSHP

Ground Source Heat Pumps (GSHPs), also known as geothermal heat pumps, are a highly efficient renewable energy technology used for both space heating and cooling in buildings. These systems have the potential to significantly reduce carbon emissions, particularly when powered by renewable electricity. GSHPs achieve this by utilizing the stable ground temperature as a heat source during winter and as a heat sink during summer, thereby decreasing the building's reliance on electricity for heating and cooling. The GSHP system, shown in Figure 1, consists of three different components as suggested by researchers [14], [15]:

- The primary unit or heat exchangers,
- The secondary unit or the piping network that delivers heat energy out or inside of the building, and
- The heat pump unit.
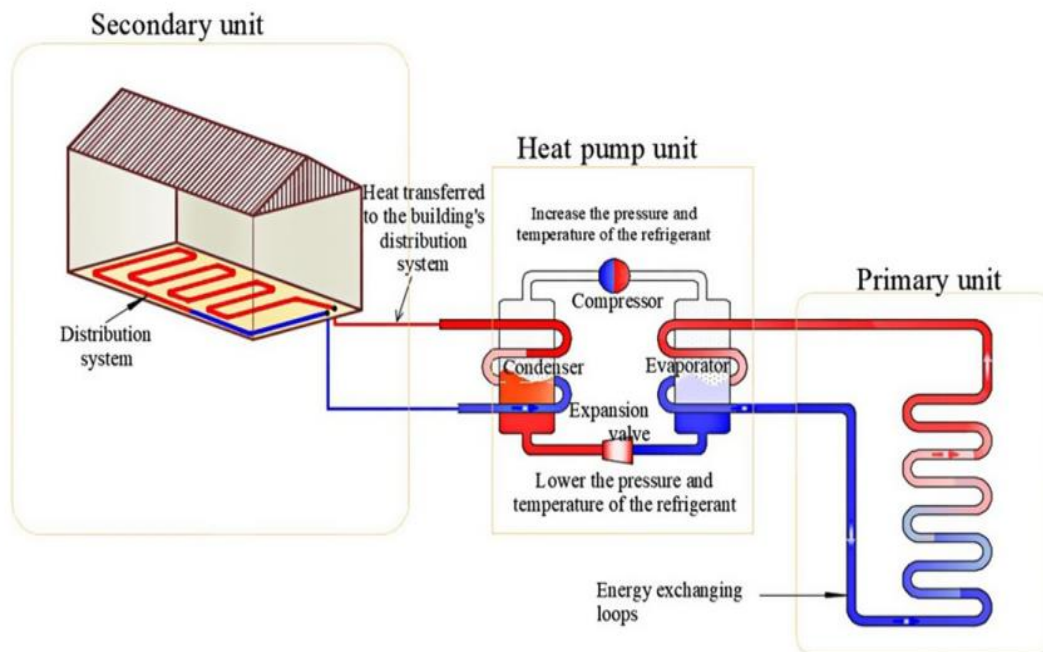
Figure 1: Ground Source Heat Pump (GSHP) system [15]

2.1.1 The Primary Unit

The primary unit, also known as the heat exchanger, comprises of different subsurface elements that help exchange heat energy with the structures above the ground surface. The elements may include base slabs, piles, and boreholes, and are fitted with energy-transferring loops or placed in direct contact with the ground using horizontal trenches.

2.1.2 The Secondary Unit

The secondary unit comprises of a closed network of pipes embedded in walls, floors, ceilings, roads, etc. It supplies the extracted heat energy from the ground to the structure to get heating or removes heat from the structure to the ground for heat storage.

2.1.3 The Heat Pump Unit

The heat pump is a mechanical device capable of increasing or decreasing the temperature of the extracted heat energy from the source. It operates in the reverse order of a refrigerator and consists of four subcomponents: the evaporator, condenser, compressor, and expansion valve, as shown in Figure 1.

For space heating, the cycle starts with pumping a constant heat carrier fluid (HCF) through the heat exchanger. The refrigerant in the evaporator retrieves the heat extracted by the HCF. The refrigerant turns into a low-pressure vapor, later fed into the compressor. The compressor compresses the low-pressure vapor into a high-temperature and high-pressure vapor, which then passes through the condenser. At the condenser, the heat energy of the hot vapor is transferred into the secondary circuit to be transferred to the building. The vapor/refrigerant condenses into liquid form, then flows to the expansion valve. The expansion valve reduces the temperature and pressure of the refrigerant, which is fed into the evaporator to restart the cycle again. On the contrary, for space cooling, the system's working principle is reversed.

2.2 Comparison of Different Types of Heat Pumps and Ground Heat Exchangers

For long-term operation, GSHPs are economical as they require less electricity demand [16]. The high efficiency of GSHPs compared to other systems can be identified based on

6

their coefficient of performance (COP). For various heating systems, the COPs are as follows: GSHPs: 3-5 (300-500%), air-source heat pumps (ASHPs): 2.3-3.5 (230-350%), electric baseboard heaters: 1 (100%), mid-efficiency natural gas furnaces: 0.78-0.82 (78-82%), and high-efficiency natural gas furnaces: 0.88-0.97 (88-97%) [17]. The efficiencies of GSHPs and ASHPs depend highly on the climates in which they operate. In a study in Greece, researchers showed that with a GSHP system, the primary energy consumption was reduced by 25.7% while the CO_2 and NOx emissions were reduced by 22.7% and 99.6%, respectively, compared to a conventional system, consisting of an oil-fired boiler and air-to-air heat pumps [18].

Ground heat exchangers (GHEs) can be classified into two types: closed-loop systems or ground-coupled systems and open-loop systems or groundwater systems, as shown in Figure 2. Open-loop systems consist of three common configurations: extraction wells, extraction and reinjection wells, and surface water systems. Among these, extraction and reinjection wells are the most common. On the other hand, closed-loop systems utilize continuous loops of pipes placed vertically or horizontally in the ground.

Horizontal GHEs, as shown in Figure 3, are formed by arranging pipes horizontally in either series or parallel configurations, and the slinky-type horizontal GHEs employ a curly arrangement to reduce ground surface area requirements. This system is easier to install and suitable when sufficient land area is available [19].

In contrast, vertical GHEs as shown in Figure 4, commonly known as borehole heat exchangers (BHEs), involve deep boreholes that allow the system to use constant and uninterrupted ground temperature for operation. This type of system is well-suited for applications where the ground area is limited, the surface landscape is rocky, the soil cover is thin, and minimal disruption to the surface is desired [19].
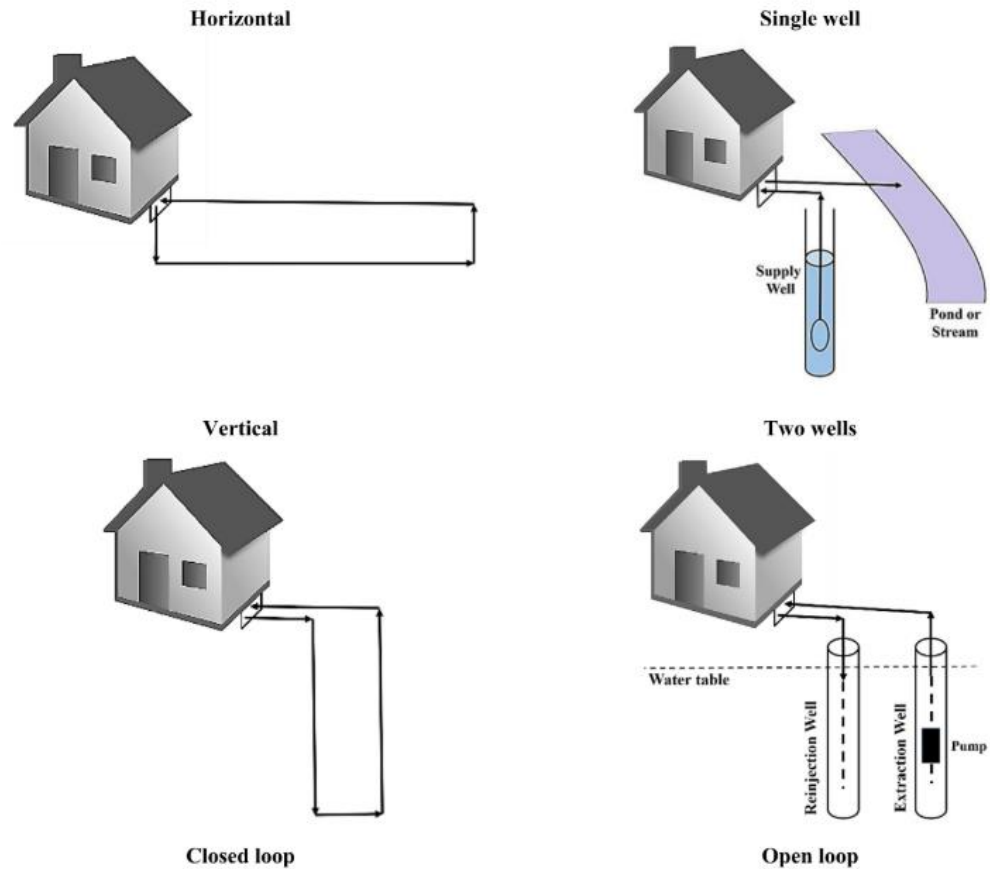
Figure 2: Closed and open geothermal loops [19]

The installation cost of Vertical GHE is more than that of horizontal GHE. However, the vertical system is more efficient for a given heating and cooling load owing to less requirement of piping, as the deep ground temperature remains warmer in winter and cooler in summer compared to the near-surface ground area [20]. As the temperature deep underground remains relatively stable throughout the year, the closed-loop system is preferred [19]. In recent years, the usage of GSHPs has increased by 10-12% [21].
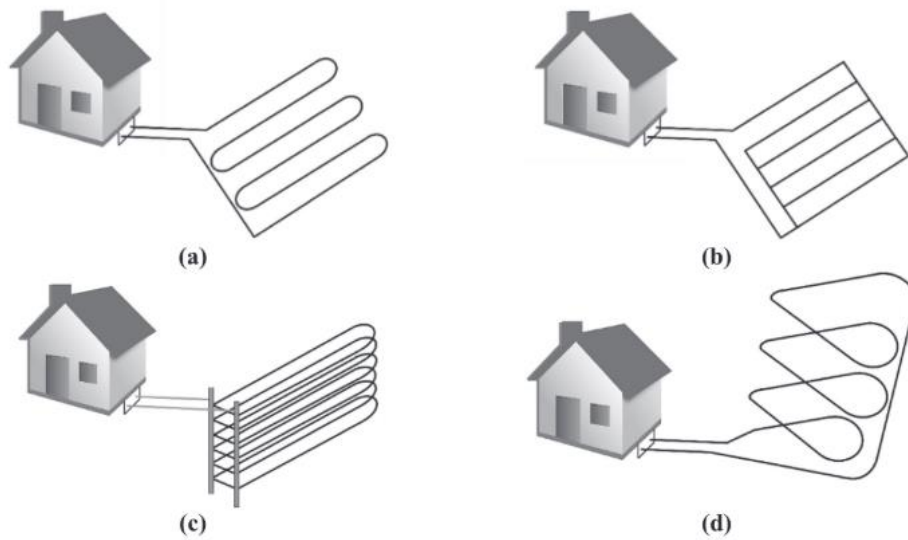
Figure 3: Various kinds of horizontal GHE (a) series, (b) parallel, (c) trench, (d) slinky [19]
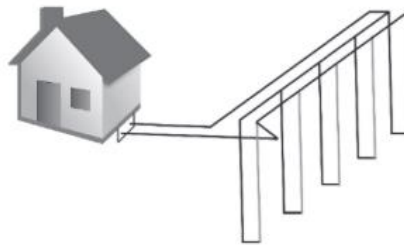
Figure 4: Vertical GHE [19]

2.3 Review of Current Studies and Description of Thermo-active Foundation

As the GSHPs show potential sources for space heating and cooling, the usage of this system has gained popularity in recent years. In China, researchers analyzed the feasibility of GSHPs in three different cities located in cold regions over one year of operation. However, their system could only handle working fluid temperatures as low as 4°C. [22]. Further investigation of the system's performance is necessary in extremely cold regions where temperatures can drop below 0°C. Bakirci [23] evaluated vertical Ground Heat Exchangers (GHE) in a cold climate in Turkey using a Borehole Heat Exchanger (BHE) of 53 m depth and an antifreeze-water mixture with a concentration of 50%. However, BHEs

involve higher drilling costs, and higher antifreeze concentrations can increase the working fluid's viscosity, leading to high-pressure losses. A study conducted in Tunisia using horizontal GHEs showed that GSHPs are suitable for operation in hot climates [24].

Despite their numerous benefits, the widespread adoption of GSHPs is hindered by their high capital cost and land area requirements [10]. Researchers have suggested coupling GSHPs with building foundations to address this issue, utilizing an existing structural element known as "Thermo-active Foundation (TAF)" to fulfill space heating, cooling, and hot water requirements. TAF eliminates the need for additional drilling costs as the GHEs are integrated within the building foundation, utilizing the same surface area, making it more economically efficient than traditional BHEs [25].

The heat exchangers in TAFs are realized by inserting pipes containing a heat transfer fluid into the building foundation piles. These piles serve a dual purpose by providing structural support and facilitating heat exchange with the ground through the flowing heat transfer fluid in the heat exchanger with the help of a GSHP coupled to the system.

The performance of the TAF system depends on various factors, including the pile foundation, working fluid, pipe material, and pipe configuration. Pile foundations can be classified as friction or bearing piles, depending on the bearing capacity mechanism. The friction pile uses the friction force around the pile, while the bearing pile is set to use the bearing load by hammering the pile head to reach the hard bearing layer [26]. The classification of TAFs also depends on the heat exchanger loop installation method and the pile material. The main types of pile materials are cast-in concrete piles, pre-stressed high-strength concrete (PHC), and steel piles [27]. Concrete is commonly used due to its high thermal conductivity and thermal storage capacity [14]. However, helical steel piles (HSPs) have gained attention recently. These piles have a hollow casing and allow drilling and installation in various types of ground materials using a welded screw and tip [28]. Energy piles are shorter and radially thicker, while the conventional boreholes are long, around 50-300 m, and radially smaller, as the energy piles require to bear the building load [27].

The choice of the working fluid plays a significant role in the GHE performance of the TAF system. The working fluid should be environmentally friendly to avoid contamination

of groundwater and biodiversity in case of any pipe leakage. Researchers have explored various working fluids, including pure water, water-ethylene glycol solution, water-propylene glycol solution, nanofluids, and other water-antifreeze mixtures. Water is the most commonly used fluid due to its availability, low cost, and excellent thermal energy storage and recovery potential [19]. However, in colder climates where temperatures drop below the freezing point of water, alternative working fluids with lower freezing temperatures are required to effectively operate GSHP systems.

Different pipe materials, such as steel, copper, polyvinyl chloride (PVC), and polyethylene (PE), have been used for GHEs. However, the impact of pipe materials on the heat exchange rate is minimal, accounting for less than 1% of the overall performance. Among these materials, PE is the most commonly used for GHE pipe loops [19].

Researchers have employed various designs for the heat exchanger loops, including Single U-pipe, Double U-pipe parallel, Double U-pipe cross, Multi-tube, Indirect double pipe, and Spiral configurations, as shown in Figure 5.
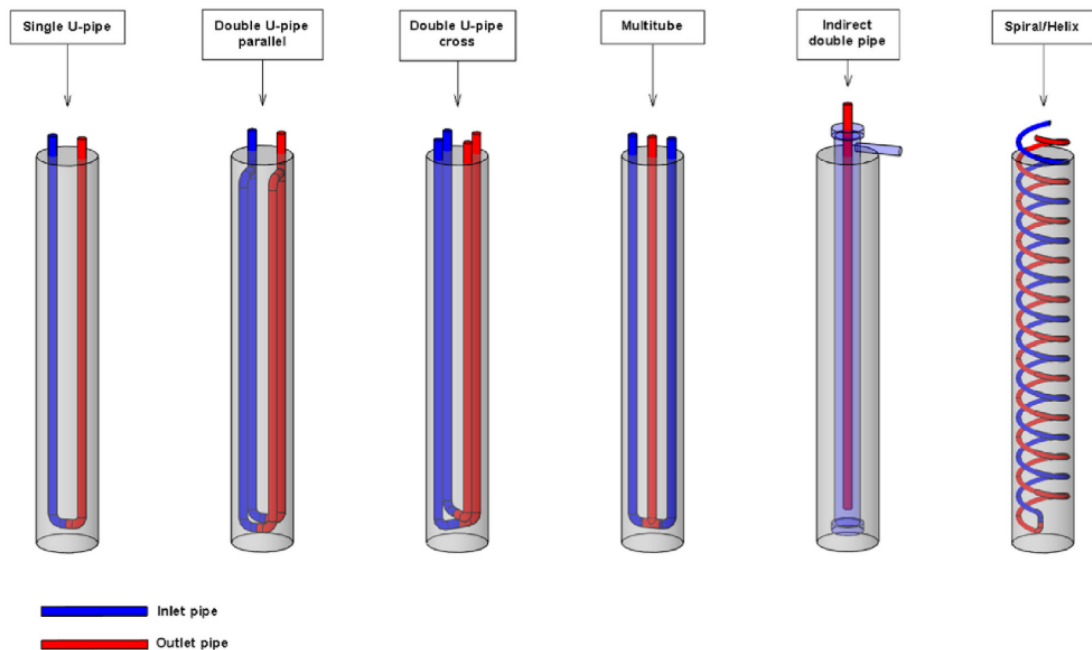
Figure 5: Vertical GHE configurations in energy piles considered by different researchers: Single U-pipe, Double U-pipe parallel, Double U-pipe cross, Multi-tube, Indirect double pipe, and Spiral, respectively [27]

11

U-tube geometries are more commonly used among the various configurations than helix, coaxial, and W-tube geometries [19]. Researchers in Japan conducted an experimental study on different types of heat exchangers in a steel pile foundation, including U-tube, double-tube, and multi-tube configurations. The study revealed that the thermal conductivity of the grout significantly influences the performance of U-tube and multi-tube heat exchangers, while the soil's thermal conductivity affects the performance of double-tube configurations [29].

While the TAF system has gained popularity among researchers in recent years, most of the analyses have focused on warmer climates, with limited studies conducted in cold climates. For example, a study at Saga University in Japan explored the performance of the TAF system under various geometric configurations in the cooling mode or summer conditions for 24 hours, using water as the working fluid [29]. Another study investigated the use of piles for a building used for both office and residential purposes, considering the heating load from mid-December to late April. However, they did not assess the system's performance in the cooling mode, which is crucial for the overall performance of GSHPs [26]. Another study investigating the thermo-mechanical behavior of energy piles under different climate conditions demonstrated that the system performs best in hot/cold-balanced climates [30]. A study done by Darbandi et al. [31] on horizontal foundation heat exchanger for cold climates shows that the system performance can improve by increasing the fluid velocity or the pipe diameter and increasing the depth of the foundation heat exchangers. Moreover, a study on slinky-type foundation heat exchangers coupled with GSHP by Davani et al. [32] for cold climates shows that, the COP of the system increases with increasing fluid velocity. Additionally, the compactness of the heat exchanger increases the performance of the system while the depth has no significant effect on the system performance for this type of foundation heat exchanger. To address the performance of vertical TAF systems in cold climates, Agarwala et al. [33] explored the performance of a helical steel TAF for one year but they didn't consider the long-term performance of the system.

As the literature shows, there are limited studies on TAF and specially the usage of TAF in cold climates over the year; it is necessary to explore the long-term performance of the

TAF with actual building loads, soil temperature, working fluid, and commercial heat pumps for cooling-dominated climates for a better understanding of the systems. Additionally, investigating the effect of different flow regimes on system performance and the impact of pile location beneath the building footprint is crucial for assessing the overall system performance.

2.4 Integration of Thermal Energy Storage in TAF

Ground thermal imbalance is another significant concern that can hinder the successful long-term operation of TAF systems. This imbalance can occur in heating-dominated or cooling-dominated climates due to an unbalanced building load. Heat extraction exceeds heat rejection into the ground over time in climates with more heating loads, while the opposite occurs in climates with more cooling loads. A stable ground temperature is crucial for the successful operation of GSHPs. Consequently, if ground thermal imbalance occurs, the ideal performance of the GSHP might fail and cause low performance of the system, resulting in lower COP and failure of the system in the long term [11]. To address this issue, additional thermal energy storage (TES) systems should be integrated into heating-dominated and cooling-dominated climates [12]. Energy storage systems are very strategic and important measures to ensure the effective usage of renewable energy and the conservation of energy. This technology can replace fossil fuels by utilizing the stored heat or cold that might be wasted otherwise [13]. Therefore, integrating TES systems with GSHP systems can effectively mitigate the thermal imbalance problems associated with unbalanced heating or cooling loads.

There are various methods for storing thermal energy, and latent heat storage is considered one of the most efficient. This method provides higher storage density, with a smaller temperature difference between storing and releasing heat, than sensible heat storage. Figure 6 shows the phase diagram of sensible and latent heat storage. For a temperature difference of 4°C from (18-20)°C and (20-22)°C in the solid and liquid phases, the total stored heat due to sensible heat is 8000 J for RT2HC PCM [34]. But for the same material, the heat stored due to latent heat is 170,000 J due to the phase change process, which is much higher than sensible heat storage. However, sensible heat storage remains the most

commonly used method for TES [35] for most applications. In GSHPs, the requirement for more stable temperatures makes latent heat storage (LTHS) attractive. Among the different LTHS systems, integrating the GSHP systems with phase change materials (PCM) is a promising solution [12].
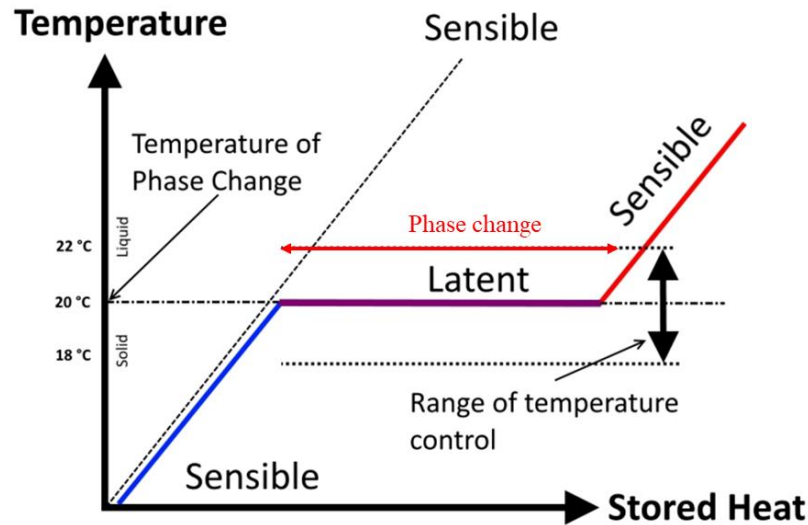
Figure 6: Sensible and latent heat storage [36]

In a review of the building materials using PCM, Baetens et al. [37] emphasized that the PCM's ability to store heat in latent form is its main property, which allows for greater heat storage capacity per unit volume compared to conventional building materials. The material will change phase from solid to liquid as the chemical bonds break up during the rise of ambient temperature. During the phase change, the materials go through an endothermic process and, as a result, will absorb heat. As ambient temperature drops, the PCM returns to the solid state and releases the stored heat. This operating principle makes PCM an ideal candidate for energy storage in GSHP systems.

TES systems using PCM must have materials with a large latent heat and high thermal conductivity. They should have a melting temperature suitable for the actual range of operation, melt compatibility with minimum subcooling and be chemically stable, cheap, nontoxic, and non-corrosive. When selecting a PCM material for any specific application, the melting temperature is the first and most important consideration [35].

There are three types of PCM - organic, inorganic, and eutectic PCM [36]. Among the available PCM materials, organic and inorganic compounds are the two most common. The summary of the PCM classification is shown in Figure 7.
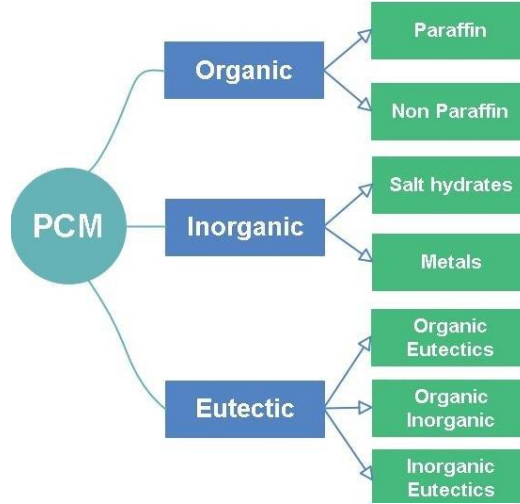
Figure 7: Types of PCM for thermal energy storage [38]

Most organic PCMs exhibit several desirable characteristics: chemical stability, non-corrosiveness, minimal or no subcooling, high latent heat per unit weight, and low vapor pressure. However, they have disadvantages such as low thermal conductivity, flammability, and significant volume changes during phase change. On the other hand, inorganic compounds offer high latent heat per unit volume, non-flammability, high thermal conductivity, and cost-effectiveness compared to organic compounds. However, their phase change properties can be affected due to their corrosive nature to most metals, suffering from decomposition and subcooling [35]. For GSHP systems, non-corrosive and non-toxic PCM materials are preferable to ensure long-term system performance. Therefore, organic PCMs are a better choice as they pose fewer environmental and system threats.

To analyze the effect of PCM on GSHP systems, researchers have conducted various studies comparing different parameters, PCM materials, and climate conditions. Michele et al. [39] investigated the coupling between PCM and flat panel type GHE through transient numerical simulations of a shallow system. Micro-encapsulated paraffin and

15

water were used as PCM, mixed with backfill materials. Comparing the performance with and without PCM, it was observed that using PCM resulted in higher surface temperatures in winter and lower temperatures in summer, leading to an increased COP of the heat pump.

Yi et al. [40] studied the combined use of PCM and compacted extended graphite as grouting material in a BHE for 40 hours. The presence of graphite enhanced heat transfer, and the PCM helped reduce temperature fluctuations in the annular and soil regions of the GHE. The COP for the cooling mode increased by 81% using PCM and 112% using graphite-enhanced PCM. However, it is important to note that these percentage changes may differ when operating for longer durations instead of just a few hours.

To enhance the heat transfer performance of GSHP systems, Kong et al.[41] studied the use of microencapsulated phase change material (MPCM) slurries as a working fluid. The results showed that utilization of MPCM slurries increased the load-to-pumping power ratio by 34% compared to water, and the COP of the GSHPs improved by up to 4.9%. However, the durability of MPCM slurries was reported to be 10.5 years in the present study, raising concerns about their long-term performance without failure. McKenna et al. [42] explored geo-cooling with a PCM tank as TES for a commercial building in cooling mode. The findings revealed that geo-cooling alone could meet 84% of the building load in 4 months, and when combined with TES, it could meet up to 99% of the load. The seasonal performance factor of geo cooling was 5.8 compared to 3.4 for the GSHP system without geo cooling.

Li et al. [43] used a shape-stabilized PCM as backfill material for a U-tube BHE with a 50 m borehole and compared its performance with crushed stone concrete. Using PCM as backfill material increased the total heat storage capacity of the BHE to 1.23 times that of crushed stone concrete, and the influence radius was 0.9 times. This suggests that the horizontal spacing between boreholes can be reduced using PCM. Additionally, the heat conductivity coefficient of PCM was found to significantly influence the coefficient of the heat pump.

Chen et al. [44] conducted an efficiency analysis of PCM grout in a U-tube heat exchanger with a 101 m borehole coupled with a GSHP, considering site conditions and dynamic load

from the heat pump. The results showed that to ensure stable operation, sustainability, and effective reduction of thermal radius; sufficient recovery time is needed for a PCM backfilled GSHP system.

Another study evaluated a PCM storage tank integrated with GSHP in a 20-year life cycle simulation for a multi-family house in a cold climate. The results indicated that there is no optimum combination of heat exchanger and PCM tank size. However, with typical drilling and PCM tank costs, the heat exchanger size can be reduced by 50% using a PCM storage tank [45].

The existing literature solidifies the benefits of using PCM as TES for GSHP systems, which enhance system performance, reduce thermal radius, decrease heat exchanger size, and mitigate temperature fluctuations in the ground for sustainable operation. However, most of the available studies are on the use of PCM in conventional BHE systems. The use of PCM for TAF systems has yet to be extensively explored.

Alavy et al. [46] conducted a numerical analysis on PCM-based energy piles with a depth of 45 m and a diameter of 1.6 m. They considered a 4 U-loop heat exchanger, where the last two U-loops were filled with PCM, totaling a mass of 655 kg. The PCM material was RT2HC, with a phase change temperature range of (1-3)°C. The study focused on a heating-dominated building load with the highest heating and cooling loads of 7.5 and 3.5 kW, respectively. The numerical simulation included the heat pump performance curve to show the instantaneous effect of PCM on system performance. The results showed that PCM demonstrated performance enhancement from December to April, with the maximum COP increase (from 3.7 to 4.3) occurring in January, corresponding to a 16% improvement in performance. Though this study shows valuable information, they didn't consider the system's long-term performance.

Shukla et al. [47] investigated the effects of PCM in a novel caisson-based energy pile with a depth of 20 m and a diameter of 1.25 m. The pile contained 13 PCM pipes filled with paraffin wax, with a melting temperature range of (5-7)°C. The experimental study spanned 28 days (from January 23 to February 23, 2020). The energy savings achieved through PCM usage in the energy pile were 2480 kWh for a heating-dominant building load, 5205

17

kWh for a cooling-dominant load, and 35 kWh for a balanced load. In the case of a heating-dominant load, energy consumption, and greenhouse gas emissions were reduced by 3% due to the 30% improvement in the thermal conductivity of PCM in both phases. The study also demonstrated that PCM reduced the thermal interference radius, allowing for more compact placement of caissons. However, it is important to note that the study considered a peak building load of 1 ton for one year, whereas actual buildings may have higher loads that could impact system performance.

Mousa et al. [48] conducted a 3D Finite Element Model simulation for an energy pile with a depth of 25 m and a diameter of 1.5 m to examine the effect of PCM on system performance. The study utilized 4 U-loop heat exchangers and 4 PCM cylinders. Two different PCMs, RT5HC and RT2HC, were tested, with temperature ranges of (4-6)°C and 1-3°C, respectively. The results indicated better performance for the PCM with the higher temperature range under their specific study conditions. The use of multiple PCM melting temperatures resulted in a 26% enhancement in performance. Additionally, the study found that the location of PCM inside the pile outperformed the outside location. The results showed a 5.2% increase in COP during PCM melting and a 1.8% reduction in COP during the solid state of PCM. The pile was buried 0.5 m underground, assuming the soil domain was exposed to ambient air. However, it is essential to investigate the effect of different pile domain locations under the building to utilize the total area under the building footprint. Moreover, while the study was conducted for one year, a long-term investigation is necessary to understand the system's performance over time.

2.5 Summary

Based on the available literature, there are limited studies on TAF for actual building loads and climate conditions for the short-term and long-term, especially in cold climates. Additionally, there is a significant research gap regarding the utilization of PCM for thermal energy storage in TAF systems. The few available studies focus on short-term studies and do not account for changing building load profiles. Therefore, this study aims to address these gaps by developing accurate models to predict the performance of TAFs in cold climates. Moreover, the potential improvements in performance using PCM are

investigated. Specifically, macro-encapsulated PCM cylinders have been employed in a helical steel pile with a U-loop heat exchanger, considering actual building load profiles, location-specific climatic conditions, and heat pump characteristics. The study includes short-term (one-year) and long-term (five-year) investigations of helical steel piles, considering their placement beneath the building's basement. Additionally, different geographic locations in Minnesota have been examined to gain insights into the impact of PCM on system performance under varying loads and climates.

Chapter 3 - Governing Equations and Numerical Modelling Procedure

3.1 Introduction

This chapter describes the numerical procedure and detailed methodology used in this study. The following sections provide the TAF's physical configuration, the assumptions used, and the governing equations. Also, the detailed boundary conditions and properties required for this study are presented.

3.2 Physical Configuration

A helical steel pile is a hollow steel casing buried in the ground with a welded screw at the tip to allow the pile to be driven into the ground. It works as a borehole heat exchanger in conventional ground source heat pump systems, but the depths are shallower (about 20 m) depending on local ground conditions, which is less than conventional borehole heat exchangers, about 60 m - 200 m, as shown in Figure 8.

A cross-linked polyethylene pipe has been inserted within the steel casing through which the working fluid flows. The space between the pipe and the steel pile is filled with backfill material to ensure heat transfer between the pipes carrying the heat transfer fluid and the ground. The soil domain surrounds the steel pile. A working fluid passes through the plastic pipe, allowing heat transfer between the heat pump and the ground.

This work incorporates a U-loop heat exchanger inside the helical steel energy pile. The pile is buried in 3 different places under a typical Minnesota small house to determine the system's capacity and long-term performance. A two-story small residential house with a basement is considered here, where the building envelope is 2028 square feet. The dimension of the building footprint is 26 ft × 26 ft. The basement wall height is 7.8 ft, the height of the floors are 9.5 ft, and an unfinished attic with a roof pitch of 6:12. These dimensions are taken from a report provided by the University of Minnesota [49] for small house configurations in Minnesota. Figure 9, 10, and 11 shows the location of the helical steel piles at different depths under the considered house including a basement which are

referred to as case-1, case-2, and case-3 consecutively. For case-1 in Figure 9 and case-2 in Figure 10, the pile is assumed to be buried under the ground at 2.4 m. For case-2, the pile is assumed to be located at the corner of the basement; for case-1, the location is under

(a) Conventional borehole heat exchanger

(b) Helical steel pile heat exchanger
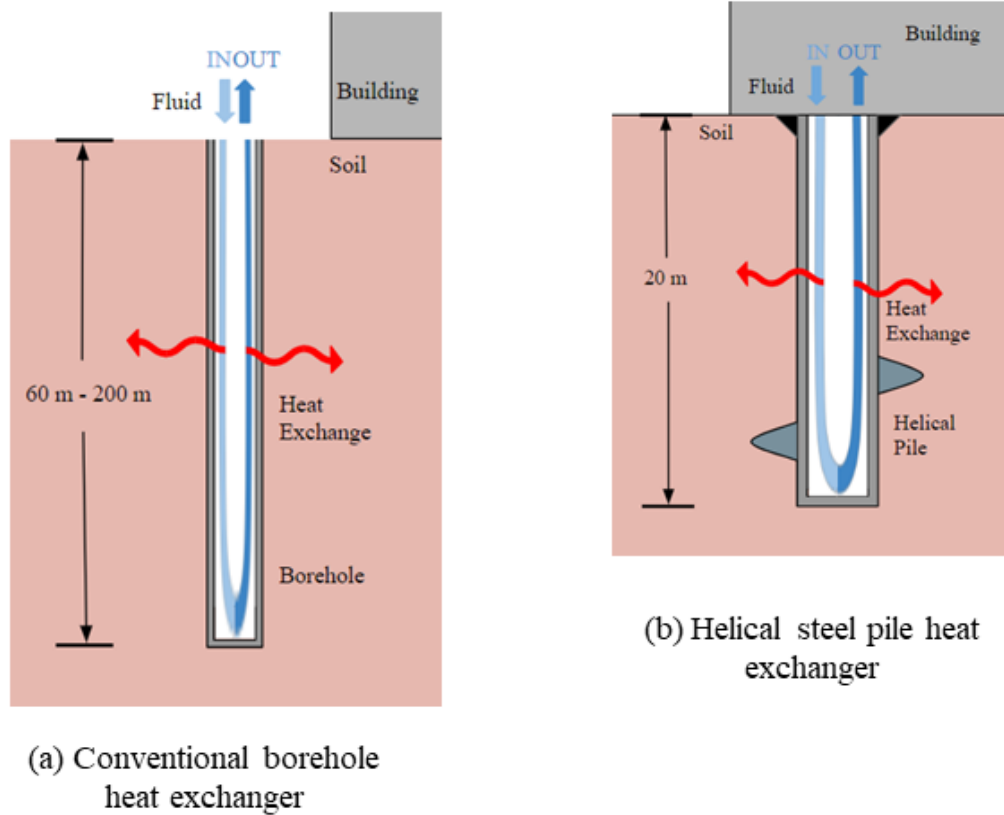
Figure 8: Comparison of (a) conventional borehole heat exchangers with (b) helical steel pile heat exchangers

the basement. Case-3 in Figure 11 is assumed to be exposed to the outdoor air. For case-3, the top of the pile is assumed to have a layer of concrete exposed to the outdoor air. For case-2, the pile is assumed to have a layer of soil and concrete consequently, which are also exposed to the outdoor air. For case-1, the top of the pile is assumed to be insulated and located under the basement at 2.4 m depth from the surface level. The layers are shown in Figure 17.

Figure 12 describes the computational domain of the steel pile used in the numerical simulations for a pile 20 m in length. The depth of the soil domain is 25 m. The parameters

21

of the pile geometry and pipe configuration are - outlet pipe diameter is 0.033 m, inner pipe diameter is 0.026 m, pipe distance is 0.02 m, and pile thickness is 0.005 m. These parameters are in line with the experimental study by Jalaluddin et al. [29].

To enhance system performance, the potential of latent heat storage using PCM is investigated. Two PCM tubes have been buried in the ground beside the pile on the left and right each, capsulated in cross-linked polyethylene. The outlet diameter of the PCM tube is 0.033 m, the inner diameter is 0.026 m, and the tube length is 20 m. Two PCM on both sides of the pile will maintain the thermal equilibrium around the pile. The distance from the PCM's center and the pile's center has been taken as 0.1 m for both PCM tubes.
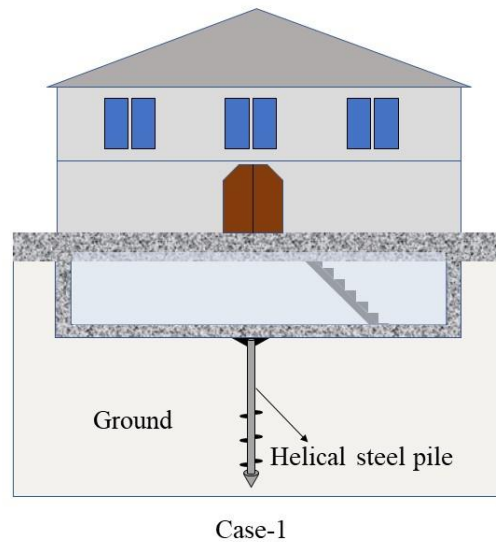
Case-1

Figure 9: Location of the pile under the basement corresponding to case-1 with the foundation
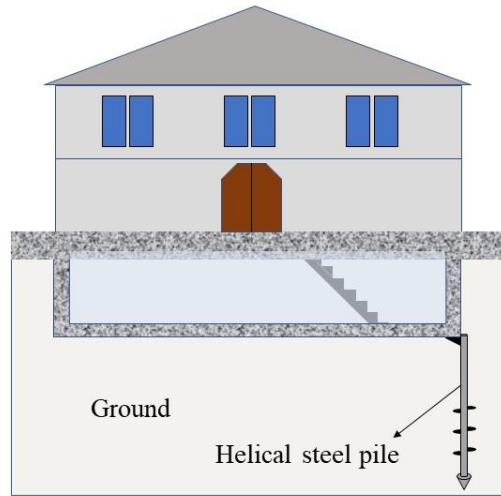
Figure 10: Location of the pile at the corner of the basement corresponding to case-2 with the foundation
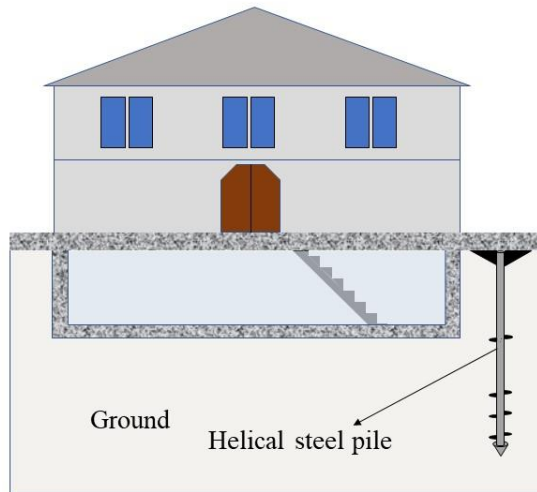
Figure 11: Location of the pile exposed to the outdoor air corresponding to case-3 with the foundation
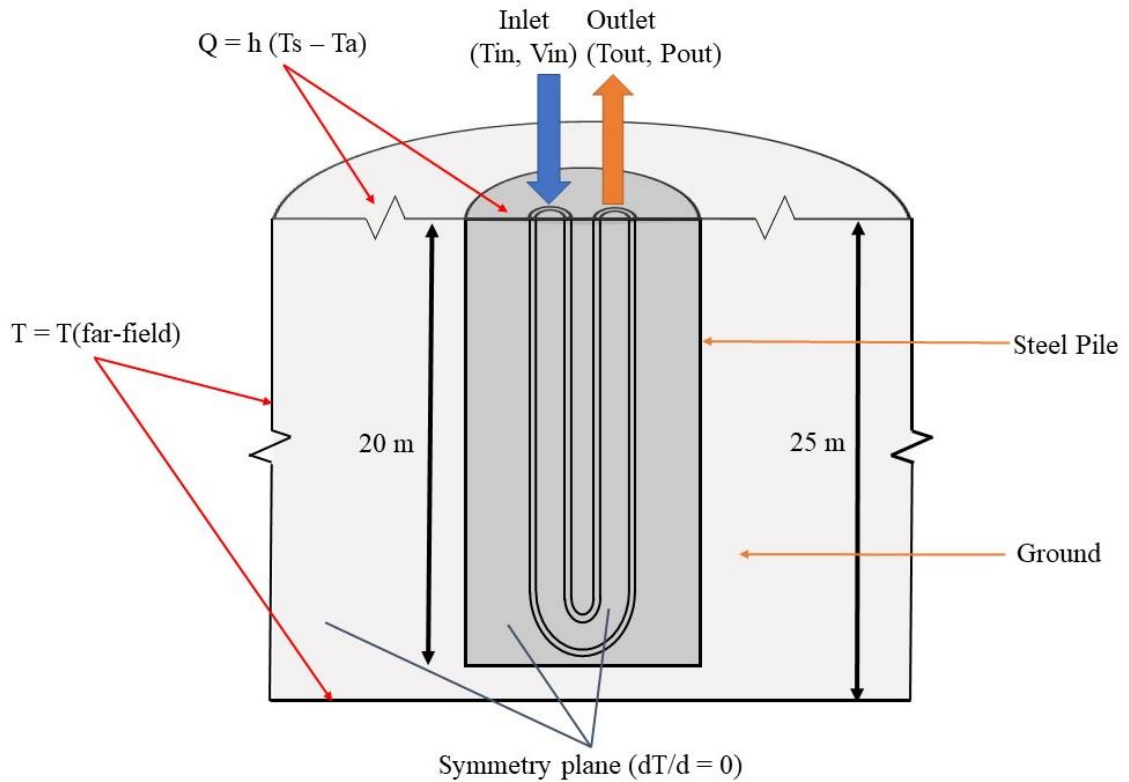
Figure 12: Schematic of the steel pile buried in the soil with the boundary conditions

3.3 Assumptions

For the long-term simulations and given the complex boundary conditions present, a number of assumptions have been made to reduce the computational cost. The pile's helix feature has not been included in the geometry, as its effect on the heat transfer performance is negligible. It can also save computational time, as suggested by some researchers [28]. The soil domain is modeled with 5 m and 10 m in diameter to model the far-field boundary condition accurately. A domain dependence study was undertaken to find the appropriate domain diameter.

3.4 Governing Equations

The fluid flowing through the U-loop inserted in the helical pile heat exchanger was considered incompressible and Newtonian. The heat transfer within the fluid happens by internal forced convection. Moreover, the heat transfer between the pipes, backfill material,

24

pile domain, and surrounding soil happens through conduction. The heat transfer in the solid regions is given by-

$$\rho_s C_{p,s} \frac{\partial T_s}{\partial t} = \boldsymbol{\nabla} \cdot (k_s \boldsymbol{\nabla} T_s) \tag{1}$$

Here, ρ_s is the density of the solid, $C_{p,s}$ is the specific heat capacity of the solid, k_s is the thermal conductivity of the solid, T_s is the temperature of the solid, and t is the time.

For the fluid flow, the continuity, momentum, and energy equations for laminar flow are solved. The continuity equation is given by-

$$\frac{\partial \rho}{\partial t} = -\rho \boldsymbol{\nabla} \cdot \boldsymbol{u} \tag{2}$$

The momentum equation is-

$$\rho \left(u \frac{\partial u}{\partial x} + v \frac{\partial u}{\partial y} + w \frac{\partial u}{\partial z} + \frac{\partial u}{\partial t} \right) = -\frac{\partial p}{\partial x} + 2\mu \frac{\partial^2 u}{\partial x^2} + \frac{\partial}{\partial y} \left(\mu \left(\frac{\partial u}{\partial y} + \frac{\partial v}{\partial x} \right) \right)$$
$$+ \frac{\partial}{\partial z} \left(\mu \left(\frac{\partial u}{\partial z} + \frac{\partial w}{\partial x} \right) \right) \tag{3}$$

$$\rho \left(u \frac{\partial v}{\partial x} + v \frac{\partial v}{\partial y} + w \frac{\partial v}{\partial z} + \frac{\partial v}{\partial t} \right) = -\frac{\partial p}{\partial y} + 2\mu \frac{\partial^2 v}{\partial y^2} + \frac{\partial}{\partial x} \left(\mu \left(\frac{\partial u}{\partial y} + \frac{\partial v}{\partial x} \right) \right)$$
$$+ \frac{\partial}{\partial z} \left(\mu \left(\frac{\partial v}{\partial z} + \frac{\partial w}{\partial x} \right) \right) \tag{4}$$

$$\rho \left(u \frac{\partial w}{\partial x} + v \frac{\partial w}{\partial y} + w \frac{\partial w}{\partial z} + \frac{\partial w}{\partial t} \right) = -\frac{\partial p}{\partial z} + 2\mu \frac{\partial^2 w}{\partial z^2} + \frac{\partial}{\partial x} \left(\mu \left(\frac{\partial u}{\partial z} + \frac{\partial w}{\partial x} \right) \right)$$
$$+ \frac{\partial}{\partial y} \left(\mu \left(\frac{\partial v}{\partial z} + \frac{\partial w}{\partial y} \right) \right) \tag{5}$$

Here, t is the time, ρ is the fluid density, p is fluid pressure, μ is the dynamic viscosity, x, y, and z are Cartesian coordinates, and the flow velocity in the x, y, and z directions are u, v, and w respectively. For equation (3-5), the left-hand side contains the local and convective fluid acceleration terms, whereas the right-hand side includes forces due to pressure, gravity, and viscous shearing forces on the fluid.

The energy equation is-

$$\rho C_p \frac{\partial T}{\partial t} + \rho C_p \boldsymbol{u} \cdot \boldsymbol{\nabla} T = -\frac{\partial p}{\partial t} + \boldsymbol{\nabla} \cdot (k \boldsymbol{\nabla} T) \tag{6}$$

The first and second terms on the left-hand side describe the local change of working fluid temperature with time and convection consequently. On the right-hand side, the first and second terms describe the pressure work and heat flux.

Equations (2) - (6) are for laminar flow. These equations will change for turbulent flow. For turbulent flow, the above equations are averaged to obtain the Reynolds Averaged Navier-Stokes equations [50]. The averaging process of these equations introduces a closure problem, requiring additional equations. The 2-equation k-ε realizable model has been used to address the closure problem in turbulence modeling [50]. The enhanced wall treatment modeling method has been applied to accurately capture the heat transfer and fluid flow in the near wall region. To ensure the proper utilization of the model, the wall y^+ value for the mesh has been evaluated as less than 1. The k represents the turbulent kinetic energy, and the ε represents the turbulent dissipation rate. The equation for k is-

$$\frac{\partial}{\partial t}(\rho k) + \frac{\partial}{\partial x_j}(\rho k u_j) = \frac{\partial}{\partial x_j}\left[\left(\mu + \frac{u_t}{\sigma_k}\right)\frac{\partial k}{\partial x_j}\right] + G_k + G_b - \rho\varepsilon - Y_M + S_k \tag{7}$$

And, the equation for ε is-

$$\frac{\partial}{\partial t}(\rho\varepsilon) + \frac{\partial}{\partial x_j}(\rho\varepsilon u_j) = \frac{\partial}{\partial x_j}\left[\left(\mu + \frac{\mu_t}{\sigma_\varepsilon}\right)\frac{\partial\varepsilon}{\partial x_j}\right] + \rho C_1 S\varepsilon - \rho C_2\frac{\varepsilon^2}{k + \sqrt{\nu\varepsilon}} + C_{1\varepsilon}\frac{\varepsilon}{k}C_{3\varepsilon}G_b$$
$$+S_\varepsilon \tag{8}$$

Where, $C_1 = \max\left[0.43, \frac{\eta}{\eta+5}\right]$, $\eta = S\frac{k}{\varepsilon}$, $S = \sqrt{2S_{ij}S_{ij}}$

In Equations (7) and (8), G_k represents the generation of turbulence kinetic energy due to the mean velocity gradients, G_b is the generation of turbulence kinetic energy due to buoyancy, Y_M represents the contribution of the fluctuating dilatation in compressible turbulence to the overall dissipation rate, C_2 and $C_{1\varepsilon}$ are constants, and σ_k and σ_ε are the turbulent Prandtl numbers for k and ε respectively. S_k and S_ε are user-defined source terms.

26

The turbulent viscosity is calculated using the following equation-

$$\mu_t = \rho C_\mu \frac{k^2}{\varepsilon} \tag{9}$$

Here, μ_t is the turbulent/eddy viscosity, and C_μ is constant.

For energy storage with PCM, the enthalpy-porosity method [50] is used to model the solification/melting process. The melt interface is not tracked explicitly in this method. But, a quantity called liquid fraction is calculated. This indicates the cell volume that is in liquid form, associated with each cell in the domain. It is computed on each iteration based on an enthalpy balance. The liquid fraction lies between 0 and 1 in a region called the mushy zone. It is modeled as a pseudo-porous medium in which the porosity reduces from 1 to 0 as the material solidifies. The porosity is zero for the solid and 1 for the liquid.

The enthalpy of the material can be written as-

$$H = h + \Delta H \tag{10}$$

Here, H is the enthalpy of the material, h is the sensible enthalpy, and ΔH is the latent heat

From equation (10), the sensible enthalpy h is-

$$h = h_{ref} + \int_{T_{ref}}^{T} C_p dT \tag{11}$$

Here, h_{ref} is the reference enthalpy, T_{ref} is the reference temperature, and C_p is the specific heat at constant pressure.

Now, the liquid fraction, β can be defined as-

$$\beta = 0 \; if \; T < T_{solidus}$$

$$\beta = 1 \; if \; T > T_{liquidus}$$

$$\beta = \frac{T - T_{solidus}}{T_{liquidus} - T_{solidus}} \; if \; T_{solidus} < T < T_{liquidus} \tag{12}$$

Equation (12) is referred to as lever rule. Here, $T_{solidus}$ is the temperature of the material is solid phase, and $T_{liquidus}$ is the temperature in the liquid phase.

The latent heat content can be written as-

$$\Delta H = \beta L \tag{13}$$

Here, L is the latent heat of the material. It can vary between zero for a solid and L for a liquid.

For solidification/melting the energy equation is-

$$\frac{\partial}{\partial t}(\rho H) + \nabla \cdot (\rho \vec{v} H) = \nabla \cdot (k \nabla T) + S \tag{14}$$

Here, H is the enthalpy from Equation (10), ρ is the density, $\vec{v}$ is the fluid velocity, and S is the source term. The solution of temperature is generally an iteration between the energy Equation (14), and the liquid fraction Equation (12).

The enthalpy-porosity method treats the mushy zone as a porous medium. The porosity in each cell is set to be equal to the liquid fraction in that cell. In fully solidified regions, the value of porosity is zero, which extinguishes the velocities in these regions. The momentum sink due to the reduced porosity in the mushy zone can be written as-

$$S = \frac{(1-\beta)^2}{(\beta^3 + \epsilon)} A_{mush}(\vec{v} - \vec{v}_{p)} \tag{15}$$

Here, β is the liquid volume fraction, ϵ is a small number (0.001) to prevent division by zero, A_{mush} is the mushy zone constant, and $\vec{v}_p$ is the pull velocity.

The analysis for PCM has been considered only for laminar velocity, so the turbulence equations has not been considered here.

3.5 Numerical Modelling Procedure

A three-dimensional transient model for the U-loop heat exchanger has been developed and analyzed to simulate the heat transfer between the GHE and the surrounding soil and

vice versa. The commercially available ANSYS Fluent software has been used, which solves the governing equations using the finite volume method [51]. Given the symmetrical nature of the flow and heat transfer, only half of the pile is modeled, as shown in Figure 12. The computational geometry is implemented in ANSYS design modeler, while the meshing is done in the ANSYS Fluent Mosaic meshing. Structured polyhedral mesh cells have been used in this work. For complex geometries, polyhedral meshing produces a smaller number of mesh cells than the traditional tetrahedral meshing, saving a significant amount of computational time. The mesh of the actual model is shown in Figure 13. To investigate potential improvements in performance with PCM, two macroencapsulated PCM has been inserted in the ground around the pile, as shown in Figure 14.
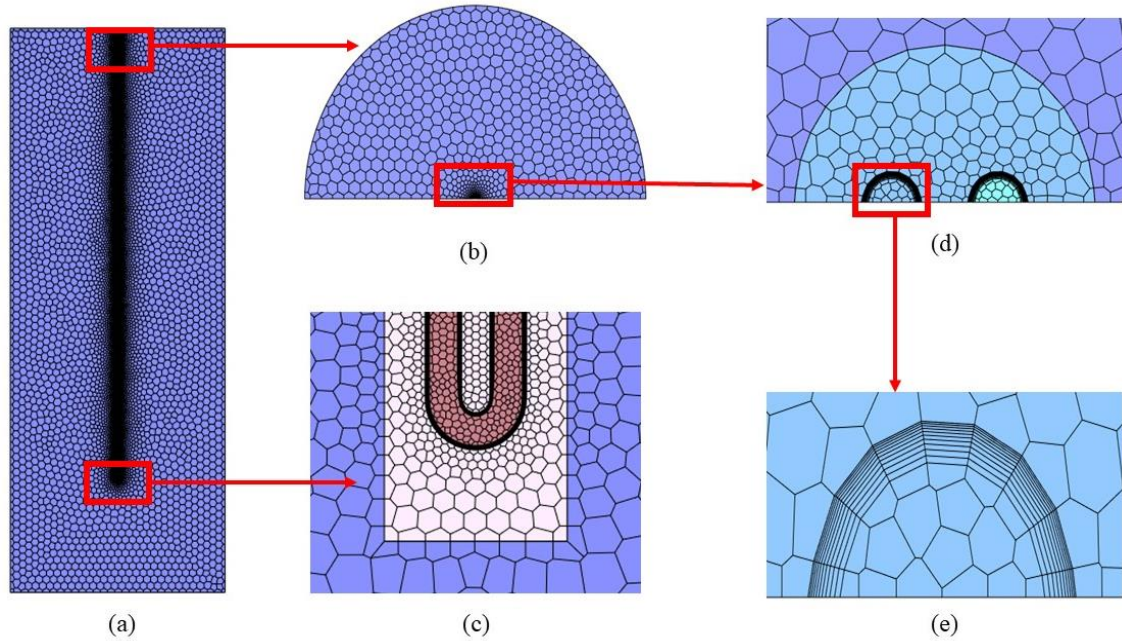
Figure 13: (a) Front view of the U-loop TAF system, (b) top view of the U-loop TAF system, (c) closed view of the U-loop, (d) closed view of the pile, and (e) closed view of inlet pipe
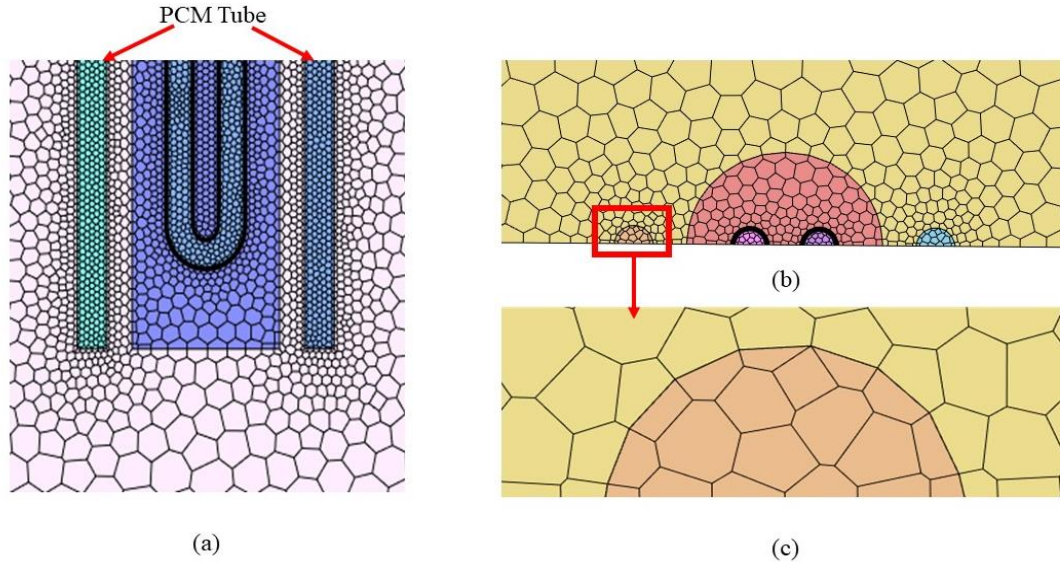
Figure 14: (a) Closed view of PCM on both sides of the helical steel pile, (b) closed view of the PCM on both sides of the pile, and (c) closed view of PCM mesh

3.6 Boundary Conditions

The boundary conditions used are shown in Figure 12. The inlet temperature is calculated from the building energy load that has been calculated using site-specific building energy modeling (BEM) for a typical small single-family house located at Duluth using BEopt [52] software - an hourly building energy modeling software. The loads were calculated on an hourly basis according to the 2012 IECC and 2015 MN energy codes representing a high-efficiency building. To calculate the loads, a single family two-story building with a basement has been considered as the typical house in Minnesota. BEopt [52] software was used for the simulation while building characteristics were extracted from a study conducted using REM/Rate software [49]. The study by Huelman et al. [49] focuses on Minnesota residential buildings.

An energy balance across the heat pump and ground heat exchanger is used to couple the building loads with the ground heat exchanger. Consequently, the inlet temperature is a time-dependent boundary condition calculated from the outlet temperature of the previous time step and the corresponding thermal load of GHE. The building energy load and the heat pump COP are used to calculate the thermal load of GHE. The inlet fluid temperature

is determined iteratively from the preceding time step using the outlet temperature using the following equation-

$$T_{f,i} = T_{f,o} + \frac{Q_{GHE}}{\rho_f C_{p,f} V_f} \tag{16}$$

Here, $T_{f,i}$ and $T_{f,o}$ are the inlet and outlet fluid temperatures, V_f is the volumetric flow rate, and Q_{GHE} is the thermal load of the ground heat exchanger.

During operation in the heating mode, the thermal load of the GHE is determined according to-

$$Q_{GHE}^{heating} = Q_{Building}\left(1 - \frac{1}{COP_{heating}}\right) \tag{17}$$

During the operation in cooling mode, the thermal load of GHEs is higher than the building energy load, which can be expressed as-

$$Q_{GHE}^{cooling} = Q_{Building}\left(1 + \frac{1}{COP_{cooling}}\right) \tag{18}$$

According to [53], the relationship between the GHEs outlet fluid temperature and the COP is assumed as-

$$COP = aT_{f,o}^2 + bT_{f,o} + c \tag{19}$$

The coefficients of Equation (19) are: a = -0.003, b = 0.056, c = 5.784 for cooling mode, and a = -0.001, b = 0.133, c = 3.257 for heating mode. These coefficient values are used for the calculations in Chapter 4.

To perform more realistic analyses, the coefficients of Equation (19) are chosen from a realist heat pump's technical data sheet for the desired conditions [54]: a = 0.003, b = -0.2879, c = 10.143 for cooling mode, and a = -0.0001, b = 0.051, c = 3.7626 for heating mode. These coefficient values are used for the calculations in Chapter 5.

To evaluate the performance of an actual helical pile heat exchanger in Duluth, International Falls, and Saint Paul in MN (our representative cold-climate locations), the

ground temperature is obtained using Xing and Spitler's two-harmonic equation [55], which is more accurate than typical Kasuda equation used for predicting ground temperature. This equation is implemented as the initial ground temperature and the far-field boundary condition. The equation is as follows-

$$T_s(z,t) = T_{s,avg} - \sum_{n=1}^{2} e^{-z\sqrt{\frac{n\pi}{\alpha_s x 365}}} T_{s,amplitude,n} \cos\left[\frac{2\pi n}{365}(t - PL_n) - z\sqrt{\frac{n\pi}{\alpha_s x 365}}\right] \quad (20)$$

Where z (m) is the soil depth, t is the time of the year starting from January 1 in days, and $\alpha_s = 0.0423$ m^2/day is the typical ground thermal diffusivity. For Duluth, International Falls, and Saint Paul consecutively, the following terms are: $T_{s,avg}$ = 278.65 K, 278.35 K, and 281.65 K are the undisturbed ground temperatures, $T_{s,amplitude,1}$ = 11.4 K,12.1 K, and 13.2 K, $T_{s,amplitude,2}$ = -1.6 K, -1.5 K, and -0.6 K, PL_1 = 34 days, 34 days, and 33 days, and PL_2 = 33 days, 25 days, and 14 days. These parameters are provided for Duluth, International Falls, and Saint Paul in MN by [55]. Figure 15 shows the far-field ground temperature profile over the year at various depths labeled as z for Duluth, MN. For the other locations, specific ground temperature profiles have been used.
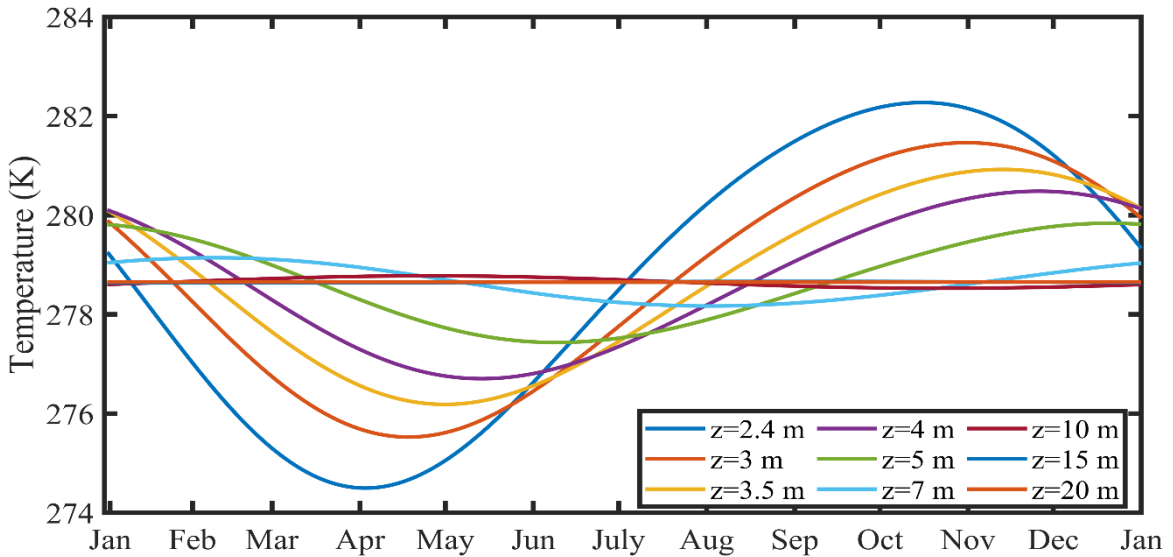
Figure 15: Ground temperature profile for Duluth, MN (far-field boundary condition)

In the simulations conducted for Duluth, MN, for case-1 in Figure 9, where the pile location is assumed under the basement, the air temperature obtained from BEopt [52] was used for the top surface, considering the air convection. For case-2 in Figure 10 and case-3 in Figure 11, the top surface convective boundary condition is computed from the transient ambient temperature of Duluth, MN for one year. The convection coefficient for air is taken as 15 $W/m^2.K$, and it validates this numerical model with the experimental study [29]. Moreover, different values for the convection coefficient were considered but there was not any significant change in the performance of the system. Figure 16 shows the basement temperature used as the convective boundary condition in case-1, and the ambient temperature used as the convective boundary condition in case-2, and case-3. For other locations, specific temperature profiles have been used for the convective boundary conditions.
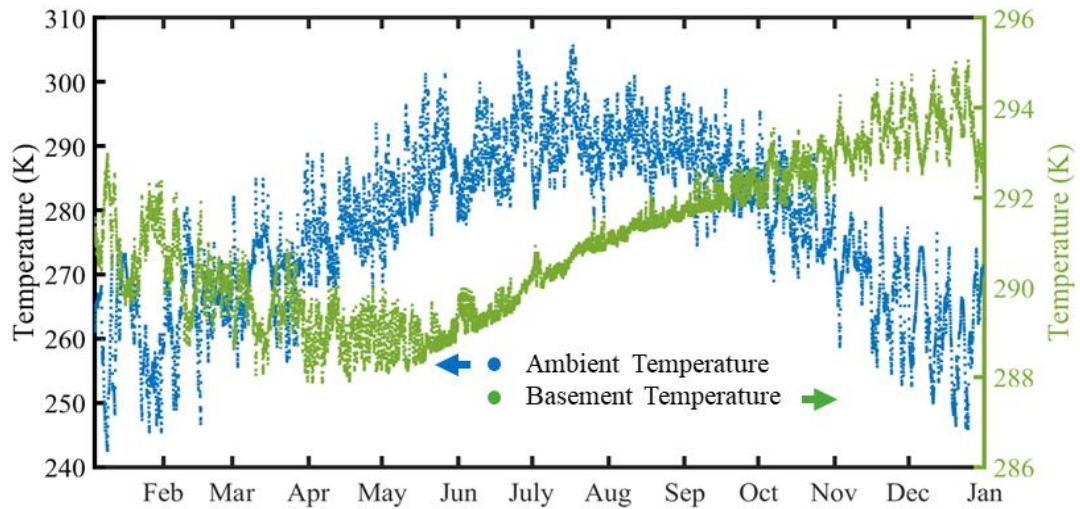
Figure 16: Ambient temperature (left-axis) and basement temperature (right-axis) for convective boundary condition for Duluth, MN

For all the long-term studies (five-year) studies, only case-1 or under the basement pile has been considered. For five-year simulations, the same boundary conditions have been used for Duluth, MN both for TAF without PCM and with PCM. For the system with PCM, the air temperature obtained from BEopt [52] was used for the top surface boundary condition considering the air convection, as shown in Figure 16.

For the five-year study of International Falls, MN and Saint Paul, MN, the same type of boundary condition has been used as Duluth, MN, but the values were different for the specific locations accordingly.

For the bottom temperature of the soil domain, the temperature is assumed to be 278.7 K, 278.4 K, and 281.7 K for Duluth, MN, International Falls, MN, and Saint Paul, MN, consecutively, calculated from the Xing-Spitler's equation at that specific depth.

For each pile location, there are specific layers between the top surface of the pile and the ambient air. For case-1, the first layer is 0.1 m of concrete; the second layer is 0.15 m of insulation; on top of it is 0.0156 m of wood exposed to the basement air. For case-2, the top of the pile is under a 2.4 m layer of soil; on top of that, another layer of 0.1 m concrete is exposed to the ambient air. For case-3, only 0.1 m of concrete stands between the pile top surface and the ambient air. Figure 9, 10, and 11 illustrates the location of case-1, case-2, and case-3 with respect to the building foundation. Figure 17 shows the layers for different cases under the building foundation.

Figure 17: Layers above steel pile at different pile locations under the building

3.7 Material Properties
3.7.1 Steel Pile Thermal Properties

The thermal properties of the steel pile and the different layers of materials over the pile used in this study are given in Table 1.

Table 1: Material Properties of the steel pile and different layers

Materials	Thermal Conductivity, K (W/m.K)	Density, ρ (kg/m^3)	Specific Heat, C_p (J/kg.K)
Cross-Linked Polyethylene	0.35	920	2174
SS400 Steel	54	7860	473
Silica Sand	1.4	2410	705
Clay	1.2	1700	1800
Concrete	1.312	2242.8	464.73
Insulation	0.0353	25	1300
Wood	0.1153	920	1214.1

3.7.2 Thermal Properties of PCM and Heat Transfer Fluid

In this study, RT2HC is used as a PCM material, and it is selected based on the desired melting temperature of PCM. A water-propylene glycol mixture has been used as the working fluid, as water freezes in colder climates as temperature drop below the freezing temperature due to the high heating loads. The concentration of propylene glycol has been taken as 25%, and the viscosity is modeled as temperature-dependent property as it highly influences the system's performance. The thermal properties of the PCM and working fluid are listed in Table 2.

Table 2: Properties of PCM and heat transfer fluid

Materials	Thermal Conductivity, K (W/m.K)	Density, ρ (kg/m^3)	Specific Heat, C_p (J/kg.K)
Propylene Glycol	0.46	1024.42	3903.3
PCM (RT2HC)	0.2	880	2000

The viscosity of a material is affected significantly by the temperature. The viscosity of a 25% mixture of water-propylene glycol mixture is taken as a temperature-dependent parameter calculated from Equation (21)-

$$\mu = 3.7307e^{-10}T^4 - 4.8277e^{-07}T^3 + 2.3453e^{-04}T^2 - 0.0507T + 4.1234 \quad (21)$$

Equation (21) is obtained by fitting data for propylene glycol at different temperatures given by [56] for 25% concentration. All the other properties of propylene glycol also have been taken from [56].

Other properties required for the PCM except from Table 2 are as follows: solidus temperature, $T_{solidus} = 274$ K, liquidus temperature, $T_{liquidus} = 276$ K, heat storage capacity $= 170,000$ J/kg, and viscosity, $\mu = 0.002377$ Pa s. All the properties of PCM excluding viscosity have been taken from [34], and the viscosity has been calculated from [57].

3.7.2 Soil Thermal Properties

The soil used for different locations in this study is a mixture of sand, silt, and clay. The properties are calculated based on their ratio in the mixture of the soil. To determine the soil properties throughout Minnesota, cities were selected based on the available weather data for the cities/towns in Minnesota taken from the town/cities' airport weather data [58]. In this study, Duluth, International Falls, and Saint Paul are the desired places in Minnesota. Obtaining the soil composition was done in two different ways:

1. Using the University of Minnesota's data [59] from a geological study giving a percentage of sand/silt/clay with depth. These were then averaged for roughly the first 80 ft since our area of interest was the first 25 m.

2. Using the United States Department of Agriculture (USDA) website [60]. With the website a specific area of interest was selected around the airport of desired location (since this was the location of the weather data). Then in the area of interest, the percentage of sand/silt/clay was estimated.

To obtain the soil moisture content, the same process of calculating soil composition from USDA [60] was repeated. The website would also estimate the soil moisture content in terms of ⅓ bar and 15 bar. According to the USDA website, the water content at ⅓ bar was used to estimate the soil moisture content as it is the most commonly used value. The percentages of sand, silt, clay, and soil moisture are shown in Table 3.

Table 3: Percentages of soil composition for different locations in Minnesota

Location	% Sand	% Silt	% Clay	% Soil Moisture
Duluth	41.817	48.183	5.863	24.3
International Falls	16.715	23.451	31.108	34.3
Saint Paul	48.266	26.290	10.688	26.3

The soil density was calculated as a weighted average given by the USDA [60] website. The soil thermal conductivity was calculated with the soil composition and the estimated moisture content at each location. The studies done by Santa et al. [61], Márquez et al. [62] have given the thermal conductivity of sand, silt, and clay individually both for dry and saturated conditions. With these properties and the known percentage of the sand, silt, and clay in the soil, the weighted average thermal conductivity has been calculated from Equation (22) - (23).

To calculate the volumetric heat capacity, the studies done by Márquez et al. [62] and Laloui et al. [63] were used to get the volumetric heat capacity of sand, silt, and clay individually both for dry and saturated conditions. With these properties and the known percentage of the sand, silt, and clay in the soil, the weighted average volumetric heat capacity was calculated from different values of the Equations (22) - (23). The dry and saturated thermal conductivity, and dry and saturated volumetric heat capacity for sand, silt, and clay are given in Table 4.

Table 4: Properties of sand, silt, and clay

Material	Dry Thermal Conductivity (W/mK)	Saturated Thermal Conductivity (W/mK)	Dry Volumetric Heat Capacity (MJ/m³K)	Saturated Volumetric Heat Capacity (MJ/m³K)
Sand	0.4	1.9	1.6	2.9
Silt	0.55	1.45	1.6	3.4
Clay	0.64	1.10	1.6	3.4

The equations used to calculate thermal conductivity and volumetric heat capacity are described below:

Dry/saturated thermal conductivity or dry/saturated volumetric heat capacity-

$$\left((0.01 * \alpha) * \lambda_{sand)}\right) + \left((0.01 * \beta) * \lambda_{silt)}\right) + \left((0.01 * \gamma) * \lambda_{clay)}\right) \qquad (22)$$

Here, α = percentage of sand per sample, λ_{sand} = dry/saturated thermal conductivity or dry/saturated volumetric heat capacity of sand, β = percentage of silt per sample, λ_{silt} = dry/saturated thermal conductivity or dry/saturated volumetric heat capacity of silt, γ =

percentage of clay per sample, and λ_{clay} = dry/saturated thermal conductivity or dry/saturated volumetric heat capacity of clay.

Now, the total thermal conductivity/ total volumetric heat capacity is given as-

$$(\Delta * \omega) + (1 - \omega) * \varphi \qquad (23)$$

Here, ω = percentage of soil moisture taken from USDA at ⅓ bar [60], φ = dry thermal conductivity/dry volumetric heat capacity, and Δ = saturated thermal conductivity/ saturated volumetric heat capacity.

Now,

$$Specific\ heat\ = \frac{total\ volumetric\ heat\ capacity}{density} \qquad (24)$$

The calculated thermal properties of the soil for different locations based on Equations (22) - (24) are given in Table 5.

Table 5: Soil thermal properties of different locations in Minnesota

Location	Thermal Conductivity, K (W/m.K)	Density, ρ (kg/m^3)	Specific Heat, C_p (J/kg.K)
Duluth	0.735	1198.16	1588.309
International Falls	0.603	1005.45	1543.906
Saint Paul	0.672	1330.27	1330.933

However, the calculated thermal conductivity underpredicts the value observed in a thermal response test in Duluth, MN done by Northern Ground Source Incorporation [64]. According to their data, the soil thermal conductivity of Duluth, MN is 1.67 W/m.K which is a lot different than the calculated data and value from the literature. To generate more realistic results based on real conditions, this value was used for all the simulations in Duluth, MN. But no thermal response data is found for International Falls, MN, and Saint Paul, MN. So, to have close to realistic values, the same thermal conductivity as Duluth, MN is used for the other two locations as their calculated values are close and comparable.

Chapter 4 - Model Validation and Performance of Non-Enhanced TAF in Cold Climatic Conditions

4.1 Introduction

In this chapter, the validation of the numerical model, the mesh dependence tests, the domain dependence tests, and effects of different flow regimes on the performance of non-enhanced TAFs, and the effects of different pile locations on system performance are presented and discussed thoroughly.

4.2 Model Validation

The developed model of the helical pile heat exchanger was thoroughly validated using available experimental data and verified by undertaking detailed mesh and domain dependence tests. Experimental data from Jalaluddin et al. [29] was used in this study. The ground temperature profile is obtained by fitting a single-harmonic equation to the experimental ground temperature provided in [29]. For the flow rates of 2, 4, and 8 L/min (0.53,1.06, and 2.12 gpm), the bottom pile and the top surface temperatures of the soil and pile are taken from the experimental study.

The outlet temperatures from the simulation were then compared with the actual experimental water outlet temperatures to validate the accuracy of our model. Figure 18 shows the experimental and present study outlet temperatures for the flow rates of 2 L/min (0.53 gpm), 4 L/min (1.06 gpm), and 8 L/min (2.12 gpm). The average percentage errors of 2.24% (+0.51℃), 1.12% (+0.27℃), and 1.05% (+0.26℃), for 2 L/min (0.53 gpm), 4 L/min (1.06 gpm), and 8 L/min (2.12 gpm) flow rates were calculated. As shown, the present study results are in good agreement with the experimental data, and they can be used for exploring the system performance under other operational conditions.
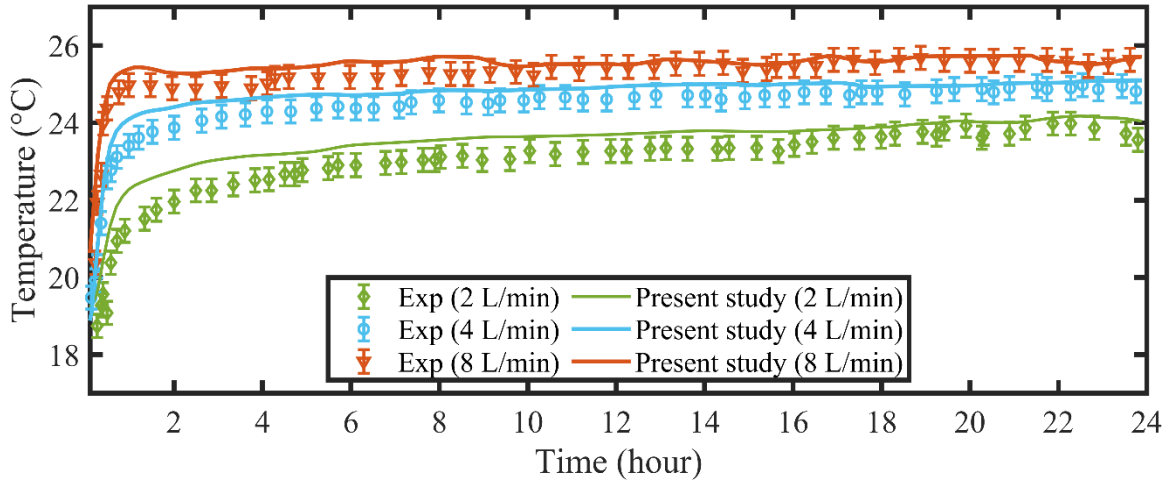
Figure 18: Validation of transient outlet water temperature at different flowrates with experimental data from Jalaluddin et al. [29]

4.2.1 Time-step Validation

For the simulations in Figure 18, the time step size was taken as 500 s, and the total simulation time was 24 hours. To check the accuracy of the time step size, a time-step verification was done for one of the flow rates, 2 L/min (0.53 gpm). For this verification, three different time steps were considered - 100 s, 300 s, and 500 s. Figure 19 shows the outlet temperatures for 24 hours for the three time steps and a flow rate of 2 L/min (0.53 gpm). The results show that the temperature is the same for all the cases. So, the choice of 500 s as the time step size is appropriate for the simulations. Besides, it also saves computational time compared to the lower time-step sizes.
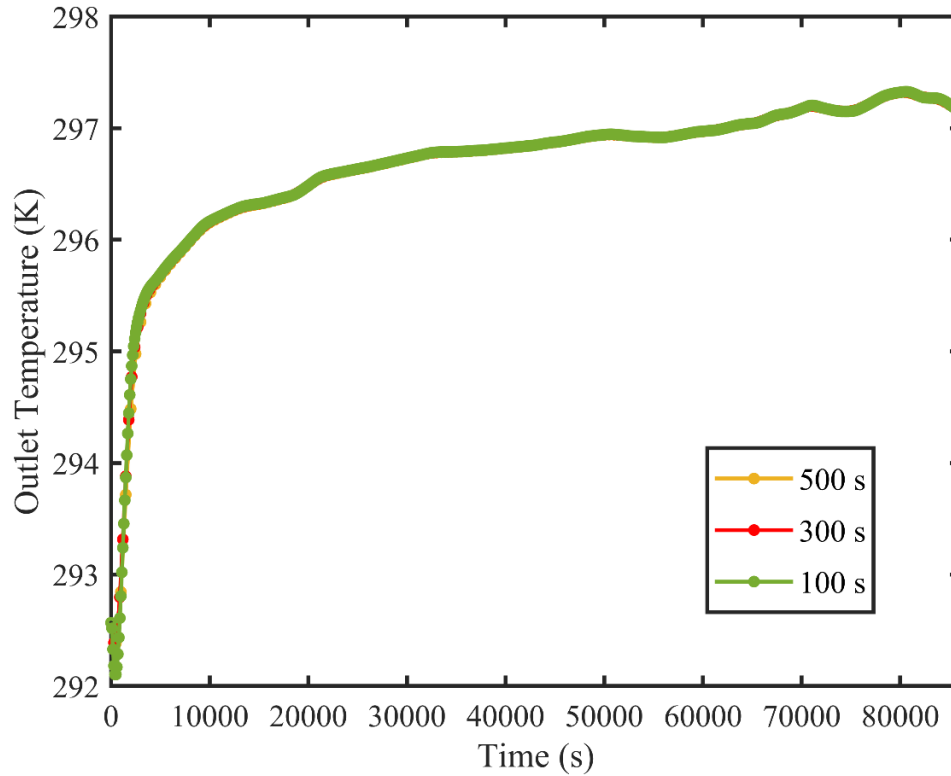
Figure 19: Time-step size validation for 2 L/min (0.53 gpm)

4.2.2 Mesh Dependence Tests

For the mesh independence study, different mesh sizes i.e., 0.5 million, 0.8 million, 1 million, 1.3 million, and 1.8 million, were used to determine the dependence of the solution on the mesh size. The friction factor and the average outlet temperature were the monitored quantities. Figure 20 shows the results of the mesh dependence test with a flow rate of 8 L/min (2.12 gpm). The average outlet temperature does not change significantly for various numbers of mesh cells. But, the friction factor gradually decreases with the increasing number of mesh cells. A mesh count of 1 million cells gives a 1.8% relative error in terms of friction factor, which is very marginal. As such, the mesh size giving 1 million cells was used in the subsequent studies to reduce the computation time without compromising the accuracy of the simulation.

41
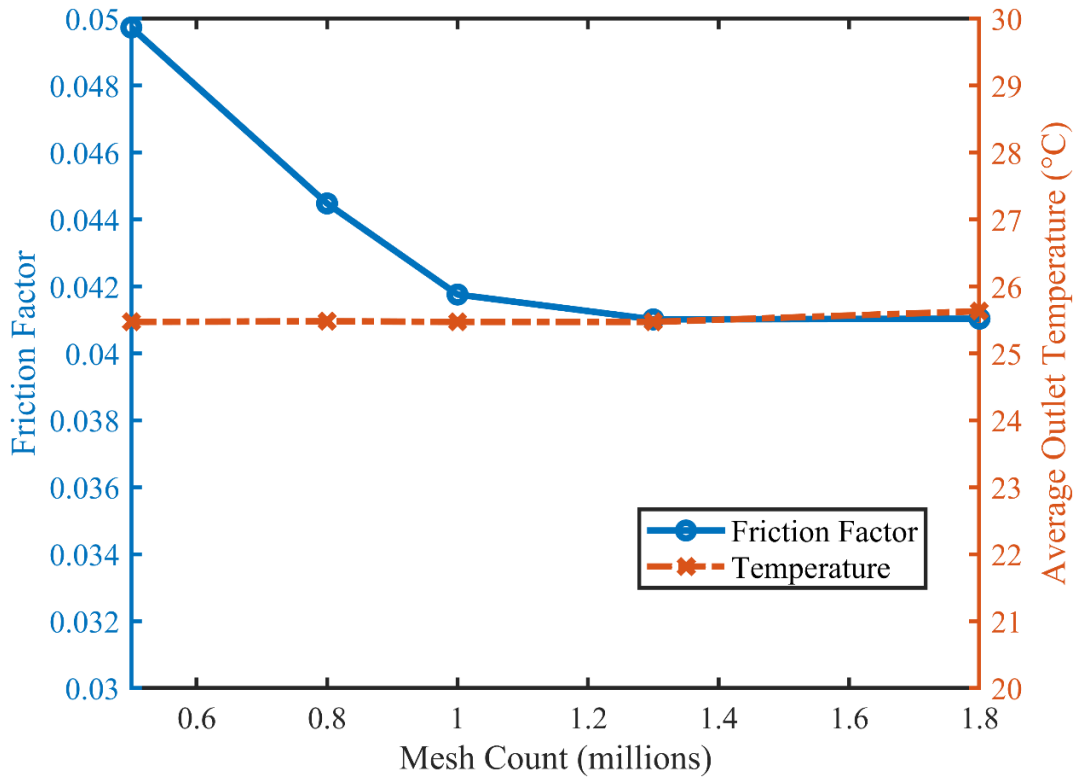
Figure 20: Mesh dependence test

4.2.3 Domain Dependence Tests

To determine the accuracy of the domain size and the applicability of the far field boundary condition used, 3 different domains were compared - 2 m diameter, 5 m diameter, and 10 m diameter. For the 10 m domain size, two refinements of the mesh were considered to capture any fluctuations in the results. In the first refinement, the mesh was coarse in the soil domain as it doesn't affect the performance of the system but increases the computational cost. In the second refinement, a finer mesh in the soil domain was created to capture any discrepancies in the whole domain. The simulations were performed for 8 L/min (2.12 gpm) and the outlet temperatures were compared and validated with the experimental study [29]. The temperatures show a similar trend for all the domain sizes. For this reason, the 5 m domain size was considered for further simulations in this chapter as it will save computational time and also will be sufficient for capturing the far-field boundary condition. In addition, soil temperature at 10 m was monitored as a means of further verification of the results. Figure 21 shows the variation of the soil temperature at

42

10 m depth for different domains. As shown, there are no significant differences between the temperatures, indicating the validity of the current results.
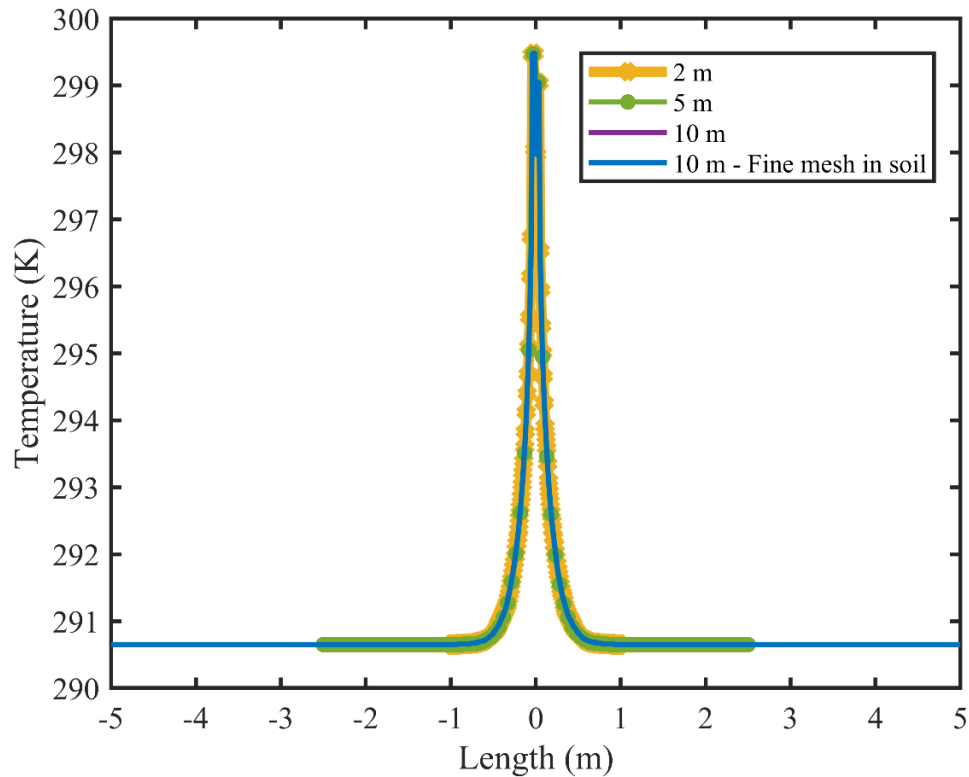
Figure 21: Domain dependence test

4.3 Parametric Results for a Non-enhanced TAF in a Cold Climate

To conduct the parametric studies for a non-enhanced TAF in a cold climate, the building load of 0.4 tons (1406 W) for a small residential house in Duluth, MN, is considered both for short-term (one-year) and long terms (five-year) numerical simulations in this section. A sample of the building load of 0.4 tons (1406 W) is shown in Figure 22 for Duluth, MN, for over one-year calculated using BEopt [52] for a typical residential small house. The loads do not change every year because the energy loads are calculated based on the requirements of the house over a year. More details about the building load in different locations are presented in the next chapter.
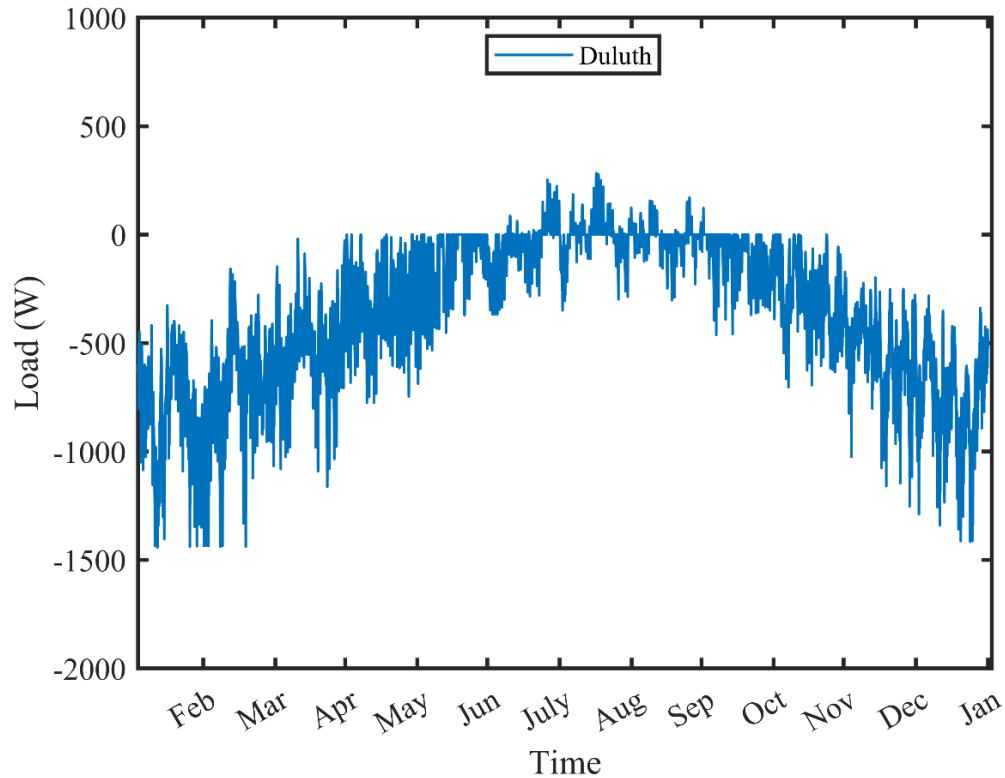
Figure 22: Sample building load 0.4 tons (1406 W) for a typical small residential building in Duluth, MN

4.3.1 Variation of Soil Temperature with Building Loads for 5 years

A five-year study based on the actual climatic and building energy loads of 0.4 tons (1406 W) for Duluth, MN and a flow rate of 1.6 m/s (13.3 gpm) velocity was done to analyze the variation of soil temperature at different radial positions from the pile. Figure 23 shows the temperatures at different radial positions (0.5 m, 1 m, 1.5 m, and 2 m) from the pile at 10 m depth from the top of the pile and shows the variation with the building load. The result shows that, near the pile at 0.5 m, the average soil temperature varies in a similar way as the building load for 5 years. However, as we move to the outer radius, the soil temperature does not vary similarly as the load varies. At much higher values of the radial position, we approach the far-field condition where the soil remains unaffected by the operation of the pile. That is why the 0.5 m point shows a similar variation with the loads, which also means that the developed model is working as intended since the soil

temperature is following the building energy load. The plot also shows that the soil temperature does not change over the years and remains constant each year.
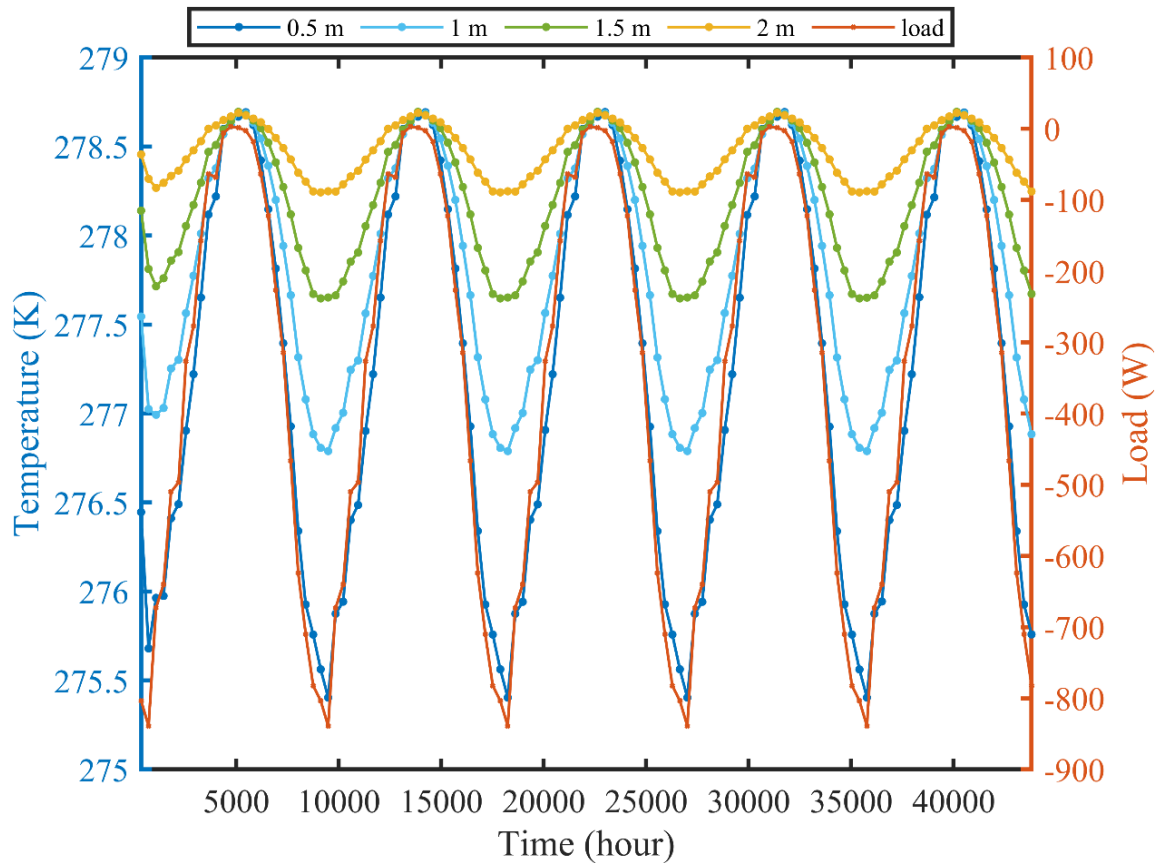
Figure 23: Variation of the soil temperature at different radial positions with the building load of 0.4 tons (1406 W) in Duluth, MN

4.3.2 Variation of the Inlet and Outlet Temperatures with the Building Energy Loads

In this study, the building energy load was reduced according to the heat exchanger's length, so that the maximum load is around 1406 W (0.4 tons). The building energy load obtained using BEopt [52] consists of both the heating and cooling loads according to the hourly building energy load. Figure 24 (a) shows the variation of energy loads in tons over the year. The negative loads indicate heating loads, while positive loads indicate cooling loads. The study starts on January 1st of a year, which is during the winter season, which is why it has a heating load at the beginning. The load ends on December 31st of a year, which is also in the winter season. The antifreeze used in this study allows the operation of GHE

45

at sub-freezing temperature, although the moisture in the soil will likely freeze in the immediate vicinity of the GHE pile at sub-freezing temperature. Reducing the building energy loads to be met by each pile to avoid a lower GHE inlet temperature can mitigate soil freezing. For a heat pump coupled with the building heat exchanger, the inlet and outlet temperatures of the helical pile heat exchanger follow the same trend as the building loads. During the heating season, the outlet temperature is higher than the inlet temperature because of the heating demand in the building, as shown in Figure 24 (b). The opposite is true during the cooling season when the building has cooling loads, as shown in Figure 24 (c).
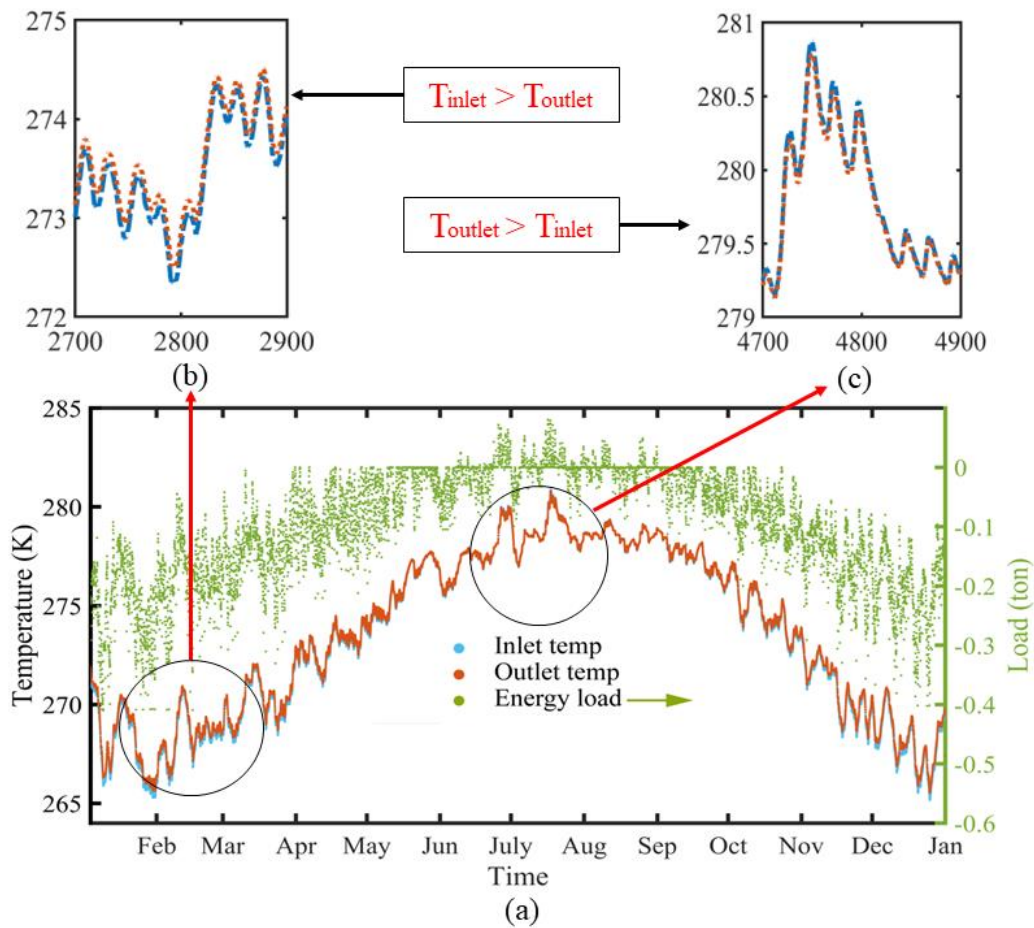
Figure 24: (a) Variation of inlet temperature and outlet temperature according to building energy loads over 1 year for (0.8 m/s) (6.65 gpm), (b) closed view of the temperatures during the heating season, and (c) closed view of the temperatures during the cooling season

4.3.3 Effects of Different Flowrates on the TAF Performance

The performance of the TAF has been considered for different flow rates representing different flow regimes for 0.4 tons (1406 W) building load over a year in Duluth, MN. Four laminar flow velocities 0.12 m/s (1 gpm), 0.2 m/s (1.67 gpm), 0.25 m/s (2.08 gpm), and 0.3 m/s (2.53 gpm) are considered for the laminar case, whereas four turbulent flow velocities of 0.8 m/s (6.65 gpm), 1.6 m/s (13.3 gpm), 2.4 m/s (19.95 gpm), and 3.2 m/s (26.6 gpm) are considered in this study. Figure 25 shows the variation of deltaT (the difference between the outlet and inlet temperatures) and pump work (the multiplication of pressure difference and volumetric flow rate) over time for different flow rates. The results show that deltaT reduces gradually with increasing velocity, and it is smaller in turbulent flow than laminar flow. The opposite happens in the pump work. The pump work increases with the velocity as it is a function of the pressure difference. With high flow rates, the pressure head in the pump is higher, which makes the pump work higher for turbulent flows, and smaller pump work for laminar flow. The lower pump work saves the power of the system.
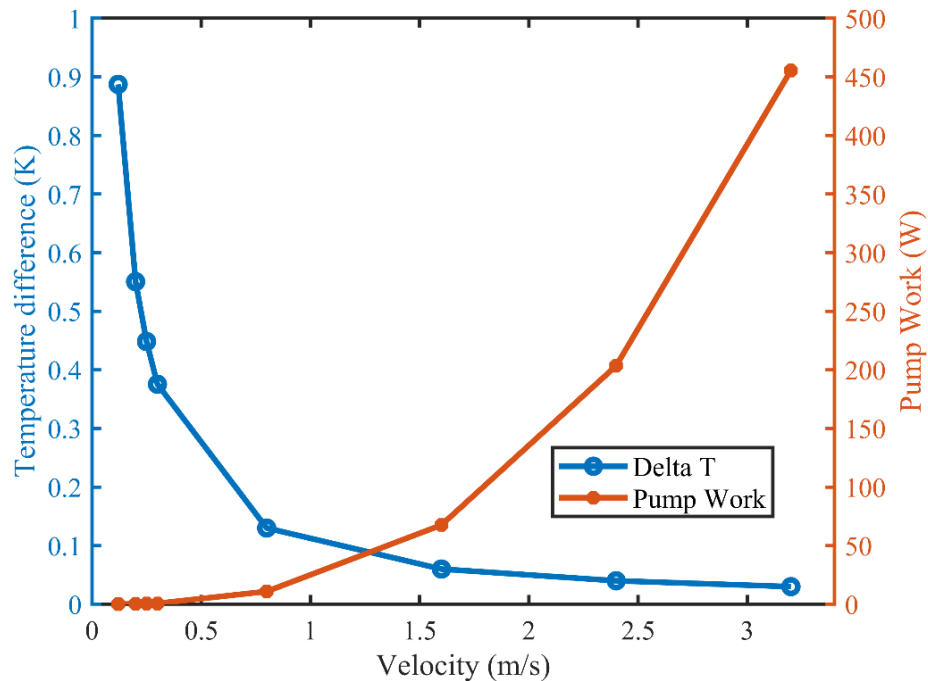
Figure 25: Variation of deltaT and pump work for different flow rates for 0.4 tons (1406 W) load over a year in Duluth, MN

47
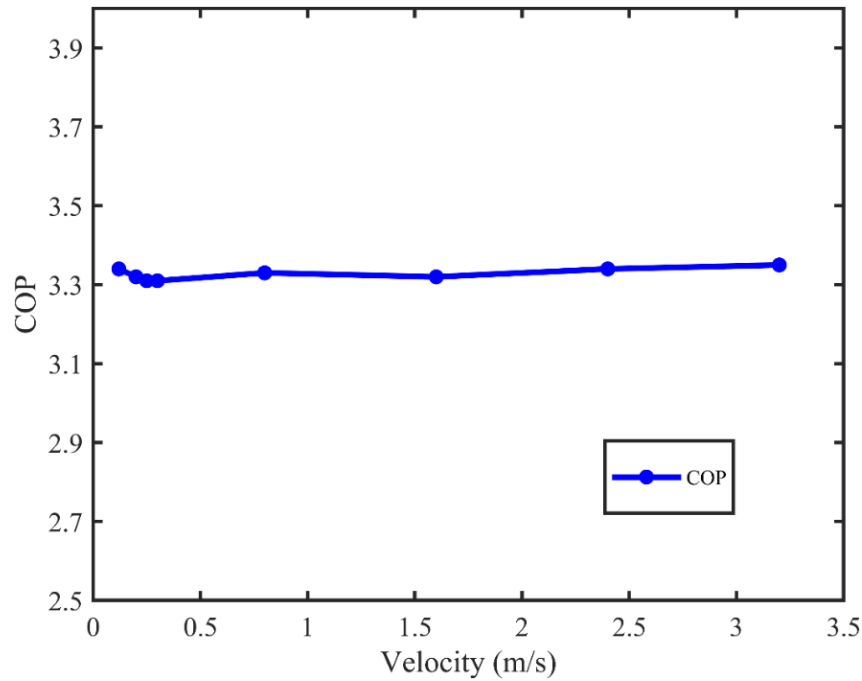
Figure 26: Variation of COP for different flow rates for 0.4 tons (1406 W) load over a year in Duluth, MN

4.3.4 Effect of Pile Location on the Performance of TAF

The influence of pile location on the COP of the system is demonstrated in Figure 27. In this figure, the COP over a period of 1 year has been shown for a turbulent flow rate of 0.8 m/s (6.65 gpm) for different pile locations, shown in Figures 9,10, and 11 for 0.4 tons (1406 W) building load in Duluth, MN. The COP of case-1 is higher than that of case-2 and case-3, during the heating season from January to May, and September to December. This is because when the pile is under the basement, the temperature inside the building is higher than the ambient temperature for case-2 and case-3. Case-2, on the contrary, has a slightly higher COP compared to case-3, as it is buried deeper in the ground, while the pile is close to the ground surface in case-3. The opposite happens during the cooling season, as the surface temperature is much hotter in summer (June to August) than in the ground. As such, the pile near the surface temperature (case-3) gives a larger value of the COP than piles in other locations. Case-1 gives the lowest COP during the cooling season. However, the average COP over the entire year for all the pile locations is around 3.3, showing that, on

average, it does not matter where the pile is located as the seasonal influences are minimum.
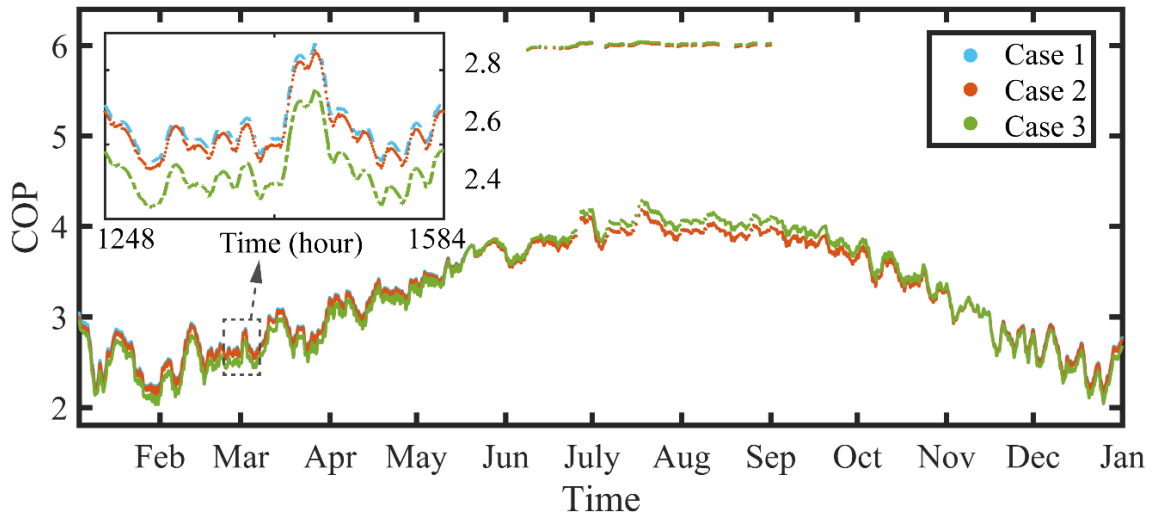
Figure 27: Variation of the COP with time for different pile locations and a velocity of 0.8 m/s (6.65 gpm) over the year for 0.4 tons (1406 W) load in Duluth, MN

4.4 Soil Temperature Distribution Over the Year

The soil temperature at lower depths near the surface changes with seasonal variations as the ambient air temperature changes over the year. But the temperatures are stable at deeper depths over the year across different seasons. In the vicinity of the TAF, it is cold in winter and hot in summer. Figure 28 shows the soil temperature variation for a computational domain of 10 m over the year in Duluth, MN. For a horizontal line at a depth of 10 m from the top of the pile across the whole domain, cutting through the U-tube pipes is used to show the temperature variation. The results in this figure are for a normalized load of 0.4 tons (1406 W). Besides, the diameter of the computational domain used in this domain is 10 m, as validated through domain independence tests. Though all the analysis in this chapter is done for a domain diameter of 5 m diameter to reduce the high computational cost, all the analysis in the next chapter is done for a 10 m domain diameter. Both of these domain size is thoroughly validated through the domain dependence tests mentioned earlier. But, the 10 m diameter domain size is mostly used and recommended by other

researchers [28], [65]. Due to that, all the analysis in the next chapter is done for a 10 m diameter domain size.

The results show that the temperature varies with the time of the year and reaches a more constant value towards the outer edge of the computational domain in line with the applied far-field boundary condition. January shows the lowest temperature (<262 K), and August shows the highest temperature, around 279 K. This variation is expected for Duluth, MN, where January is in the winter season and August is in the summer season.
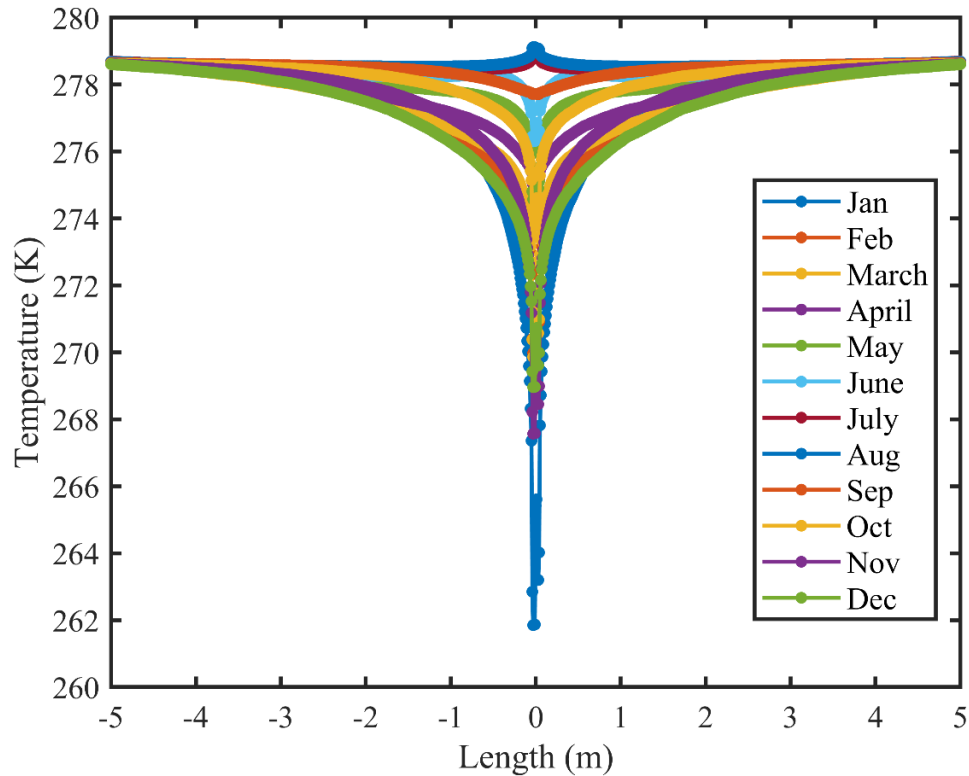
Figure 28: Soil temperature for 10 m diameter domain at a depth of 10 m for a normalized building load of 0.4 tons (1406 W) for a typical small residential building in Duluth, MN

4.5 Summary

In this chapter, the non-enhanced TAF numerical model is thoroughly validated and verified with an experimental study. Detailed mesh dependence tests, time-step verification, and domain dependence tests have been done to further verify the model and the far-field boundary condition. Different parametric studies have been done for a small

residential house in Duluth, MN of 0.4 tons (1406 W) normalized building load. The results show that laminar flow with a lower flow rate is a better choice for the pump operation, as it saves pump power but gives the same average COP of around 3.3 with higher flow rates. Moreover, the TAF performance is not dependent on the pile location, as for different pile locations under the building footprint it gives the same average COP of 3.3.

Chapter 5 - Performance Enhancement of TAFs Using Latent Thermal Energy Storage

5.1 Introduction

This chapter explores the performance enhancement of the thermo-active foundation (TAF) using latent thermal energy storage with PCMs. The potential of enhanced TAFs to meet different magnitudes of the building energy loads for a typical small family residence in Duluth is analyzed. Long-term performance results (five years) are then used to determine the optimum load in each pile that the TAF can satisfy over the years and is economically beneficial. The soil temperatures at different times of the year are also evaluated to show the variation in different seasons, both at non-enhanced and enhanced conditions.

After selecting the optimum load capacity of each pile, the performance of the TAF has been explored for the other two locations in Minnesota i.e., International Falls and Saint Paul to analyze performance in different climate conditions in Minnesota. The performance of the enhanced TAF at these locations has been compared with that of a pile in Duluth, MN to compare the performance in different climatic conditions. In this chapter, a flowrate of 0.12 m/s (1 gpm) was used for all studies. As shown in Chapter 4, lower flowrates corresponding to the laminar flow regime result in lower pumping power requirements enhancing the system efficiency. Moreover, generally, the heat pump requires a 3 gpm flowrate for 1 ton of building load. To calculate the COP, the coefficients of Equation (19) were calculated from a realist heat pump's technical data sheet [54]. All the analysis in this chapter is done using a soil domain of 10 m diameter to accurately model the far-field boundary condition and to maintain a more realistic approach with existing literature.

5.2 Enhancement of the TAF Performance Using PCM

The enhancement of ground source heat pump systems using PCM for latent thermal energy storage is considered an attractive option, given the ability of the PCM to keep ground temperatures more stable during the phase change process. Although several studies have looked at the enhancement of conventional borehole heat exchangers using

PCM, there are limited studies on the use of PCM in helical pile based TAFs. This section discusses the influence of PCM on the long-term performance of a helical pile TAF in a cold climate.

5.2.1 Long-term Performance Analysis of TAF Using PCM

A long-term study over five years has been undertaken for Duluth, MN using a normalized building energy load of 0.4 tons (1406 W) as the maximum load for cases with and without PCM. Figure 29 shows the outlet temperature of the heat exchanger over five years with and without PCM and the entering water temperature (EWT). The entering water temperature is the minimum value above which the heat pump operates successfully. For the pump used in this study, the lowest allowed entering water temperature (EWT) is 268.15 K. Below this temperature, the pump will shut down. As such, another means of heating is needed to ensure comfort conditions are met. The results show that, without PCM, the system temperature drops more times of the year below the lowest EWT, but after using PCM, the outlet temperature of the TAF rises slightly and drops less times below the lowest EWT. The PCM stores energy through the latent heat of phase change and the charging and discharging of the PCM helps to maintain the ground temperature at a higher temperature, which keeps the outlet temperature of the system higher than the case without PCM. In this study, the temperature drops below minimum heat pump EWT 14.58% of the time or needs additional heating for 14.58% of the time in one year without using PCM, but it drops to only 6.30% or requires additional heating for only 6.30% of the year with the incorporation of PCM.

Therefore, the PCM helps to enhance the performance by 8.28% in a year or requires additional heating by 8.28% less in a year than without PCM. As such, the system will need additional heating only 23 days a year after using PCM instead of 53.2 days. Results also show that the outlet temperature does not change after the second year for the rest of the years considered for both cases with and without PCM. There are some variations in the first year and second year as the system takes some time to adjust completely with the boundary conditions and the physics for a transient study. As the temperature does not change after the second year, to reduce the computational cost, the other analyses in this

chapter are done for only two years in further simulations to capture and predict the long-term performance of different building loads and different locations.
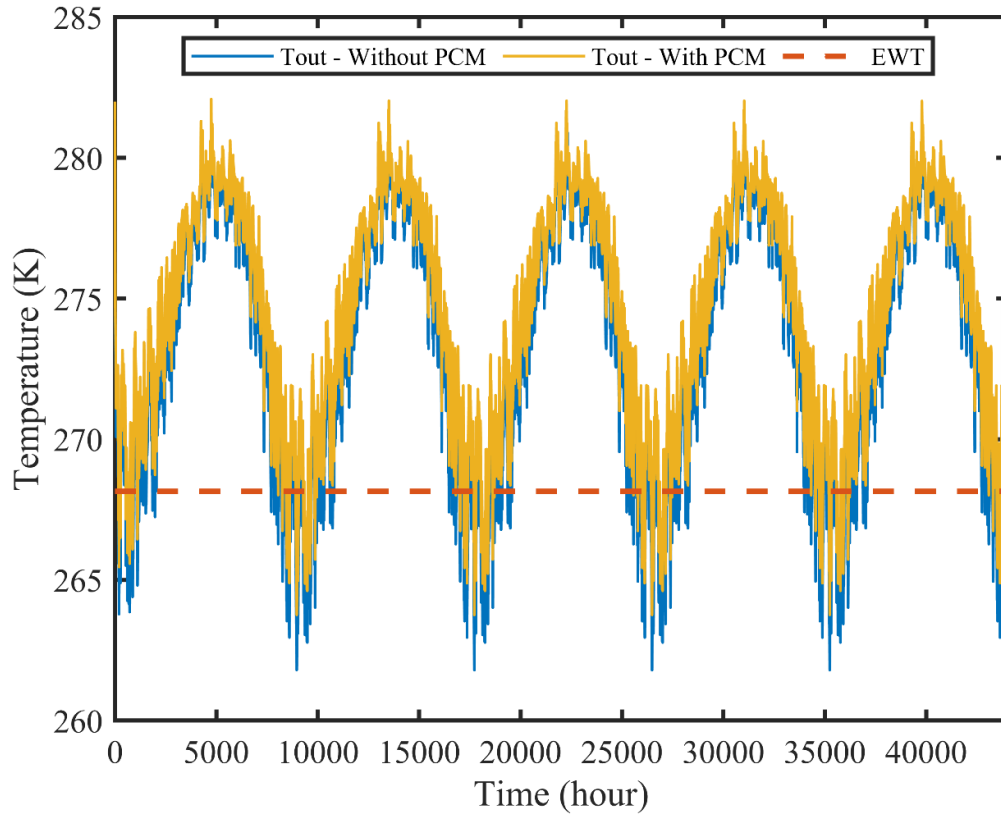
Figure 29: U-loop outlet temperature with and without using PCM for 5 years and entering water temperature of the heat pump for 0.4 tons (1406 W) load in a small residential building in Duluth, MN

5.2.2 PCM Temperature and Liquid Fraction

In this study, the PCM melting temperature range was (1-3)°C. The solidus temperature of PCM was 274 K or around 1°C, and the liquidus temperature was 276 K or 3°C based on the average temperature without enhancements in Figure 29. The PCM for these temperature ranges is available from the Rubitherm Technologies GmbH [34]. It means that PCM will start to solidify below 274 K, and the liquid fraction will reach 0 when it completely solidifies. On the other hand, the PCM will start to liquidify after 276 K, and the liquid fraction will approach to 1 when it fully liquidifies. Figure 30 shows the average PCM temperature on the left-y axis and liquid fraction on the right-y axis for one year,

starting from January to December, for a normalized building of 0.4 tons for a typical small residential house in Duluth, MN. It shows that, in the beginning, the PCM is liquid, but as the temperature drops at the beginning of the year, it starts to solidify and reaches a fully solid phase, as shown by a liquid fraction of 0. Around February, complete solidification happens, making the liquid fraction completely 0. After some time, the PCM temperature starts to rise around March as the heating demand gradually reduces during the year. The liquid fraction increases to values above 0, indicating partial melting. During the summer season, around May, the temperature starts to rise above 274 K and surpasses 276 K, completely melting the PCM. The liquid fraction approaches 1 and becomes fully liquified from May to the start of November and stores latent heat during this time which will help to enhance the performance in the next season of the year. From November, the PCM temperature again drops with the start of the winter season and high heating demands, which also reduces the liquid fraction values below 1, and reaches 0 at the end of December.
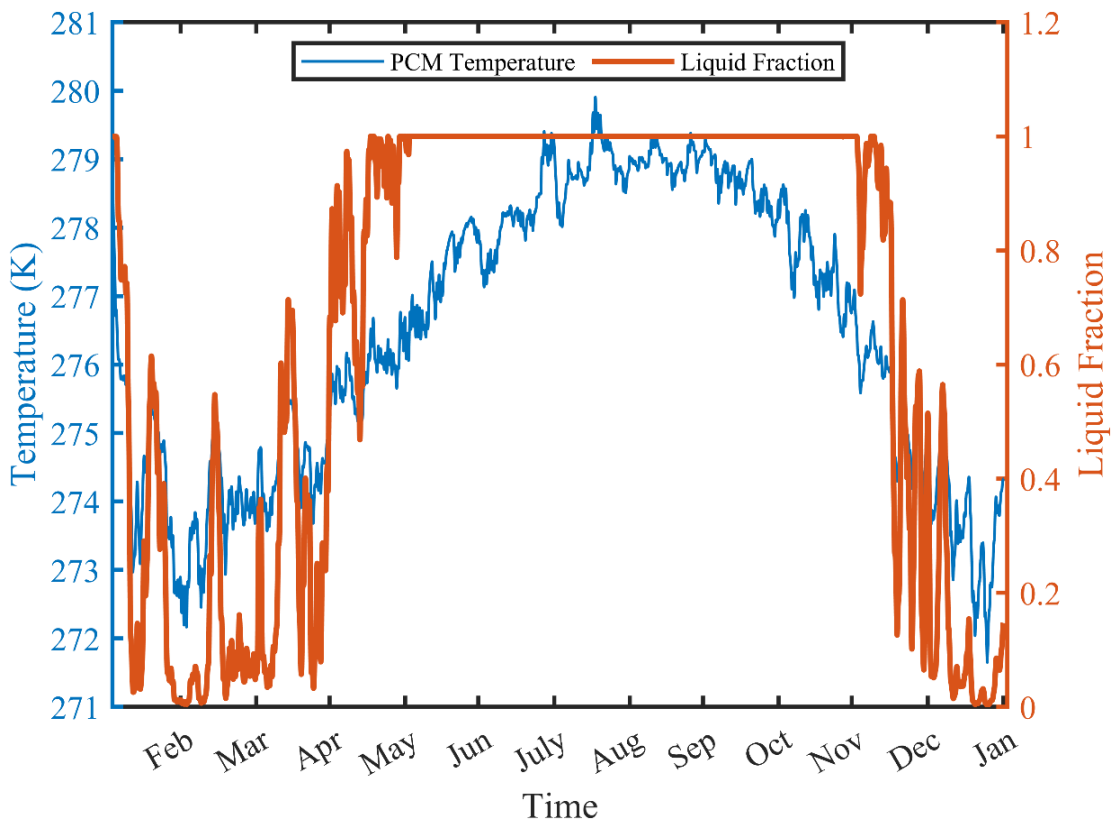
Figure 30: Average PCM temperature (left-axis) and PCM liquid fraction (right-axis) for 0.4 tons (1406 W) of load in Duluth, MN for 1-year

5.2.3 COP for 0.4 tons with and without PCM for Duluth, MN

The COP for the heat pump coupled with the TAF for cases with and without PCM was evaluated for Duluth, MN, for a normalized building energy load of 0.4 tons (1406 W). Figure 31 shows the COP for one year. As the figure shows, the heating COP during winter is slightly higher for the case with PCM than the case without PCM. The average annual heating COP is 3.72 without PCM and 3.78 with PCM. The addition of PCM ensures a more consistent heat pump entering water temperature as the PCM solidifies during latent thermal energy storage in the heating season or winter.

On the other hand, the average cooling COP during summer is 8.48 without PCM and 8.37 with PCM. The summer COP drops for the case with PCM because of the warmer ground temperatures due to the PCM's stored energy, which reduces the capability of the heat exchanger to discharge more heat in the ground to have a better cooling effect. As a result, the cooling effect drops a bit, and the outlet temperature of the ground heat exchanger gets higher, resulting in a lower cooling COP. The annual average COP without PCM is 4.05 and 4.09 with PCM, which is very close despite the slight differences in the seasonal COPs. The average long-term COP for over five years is 4.03 without PCM and 4.08 with PCM.
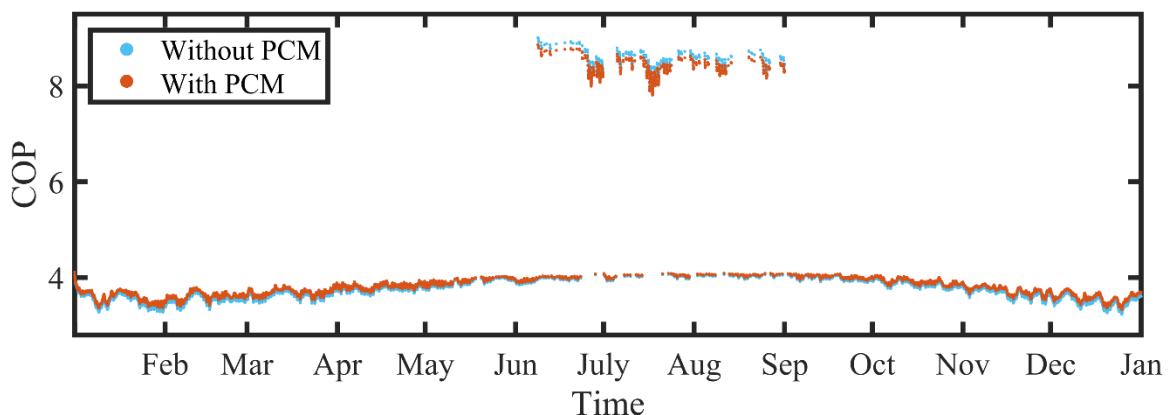
Figure 31: Heat pump COP for a TAF with and without PCM in Duluth, MN for 1 year and a normalized building load of 0.4 tons (1406 W)

5.3 Soil Temperatures at Different Times of the Year with and without PCM

Based on the previous discussions, we know that the soil temperature varies over the year in different seasons and that using PCM helps enhance the performance by ensuring small soil temperature changes. Figure 32 shows the soil temperature along a line at a depth of 10 m from the surface across the whole domain with and without PCM in January. The results show that the outlet temperature drops below 262 K in January, indicating the cold temperatures as heat is extracted from the ground during winter. Moreover, much lower temperatures are in the vicinity of the pile. The figure also shows that the temperature using PCM is higher than the temperature without PCM, which means it helps to enhance the performance, as the stored energy in PCM helps to increase the ground temperature slightly, resulting in higher outlet temperatures in winter.

Figure 33 shows the soil temperature along a line at a depth of 10 m from the surface across the whole domain with and without PCM in April. The temperatures are greater here than in January since the ambient temperature is higher in April, leading to lower heating loads and, therefore, less energy extraction from the ground. This makes the ground temperature higher than January's and the outlet temperature more than 274 K, which is above the freezing temperature.

Figure 33: Ground temperature in April with and without PCM for a TAF with a
normalized load of 0.4 tons (1406 W) in Duluth, MN

Figure 34 shows the soil temperature along a line at a depth of 10 m from the surface across the whole domain with and without PCM in July. The temperatures are higher here than in April as the ambient temperature goes much higher in July, which is also the summer season. There is no heating requirement here but there is a cooling requirement. The results

show that the outlet temperatures are above 278 K, which is a lot warmer than January and April.
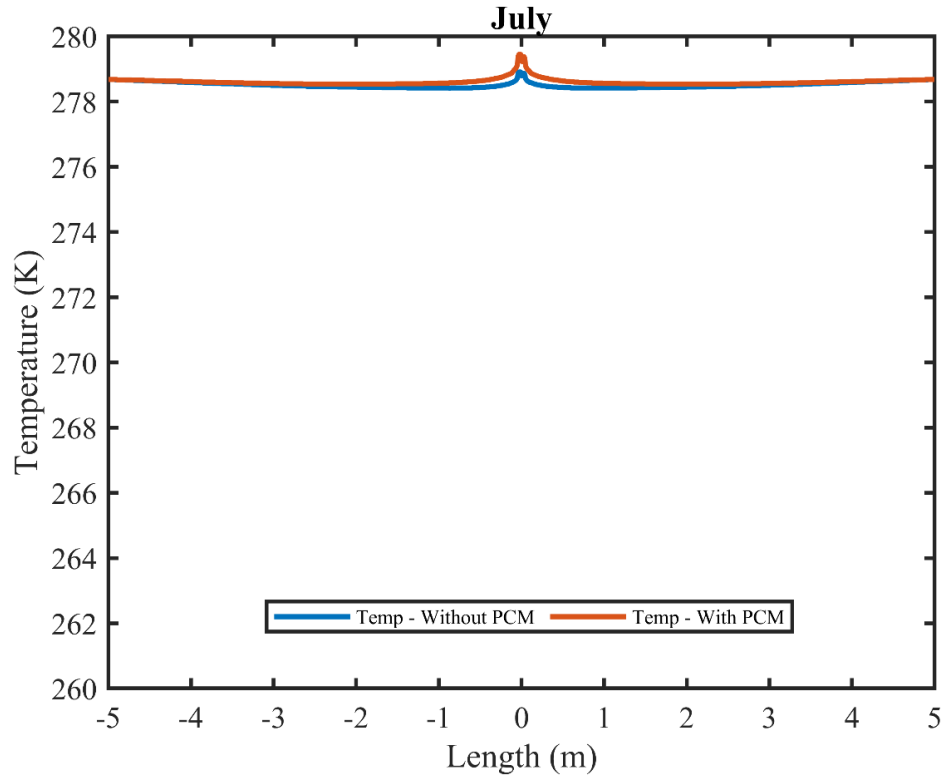
Figure 34: Ground temperature in July with and without PCM for a TAF with a normalized load of 0.4 tons (1406 W) in Duluth, MN

Figure 35 shows the soil temperature along a line at a depth of 10 m from the surface across the whole domain with and without PCM in October. The temperatures are lower than in July as the ambient temperature is lower in October than in the summer, which is July. The temperature drops below 274 K, which means that there is again heating requirements needed, and the PCM is helping to get a slightly higher temperature by storing energy which increases the ground temperature.
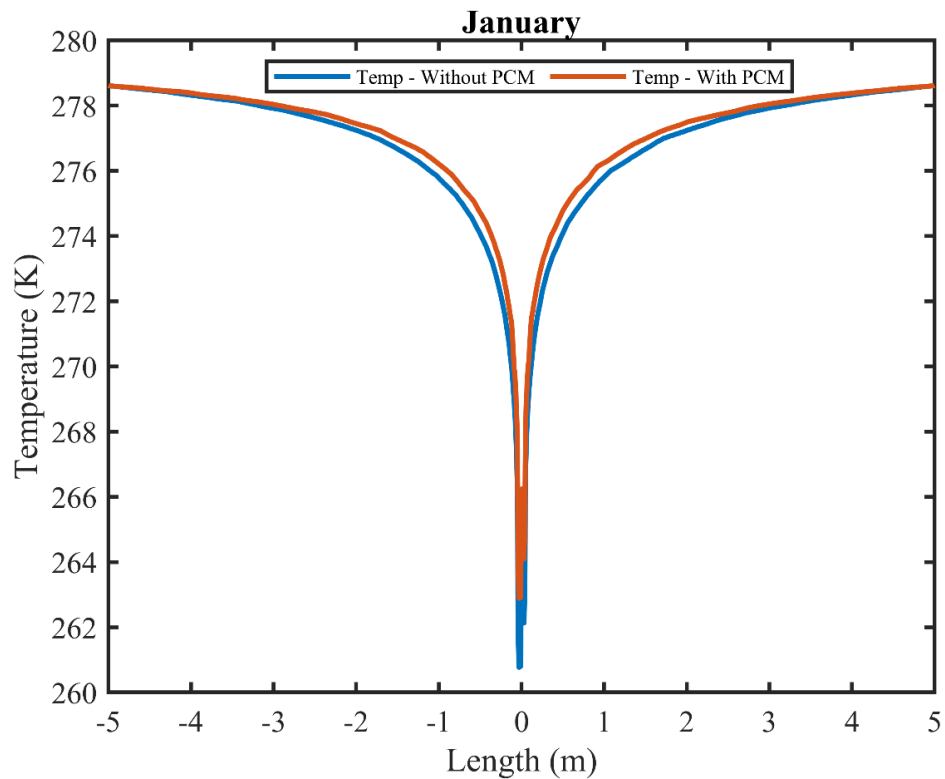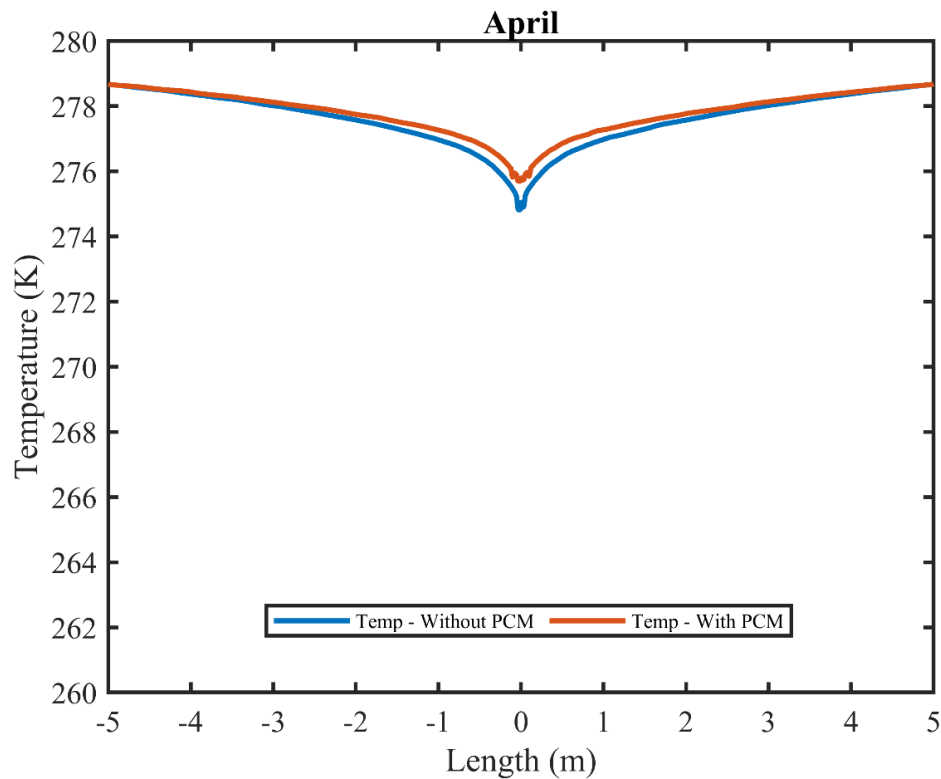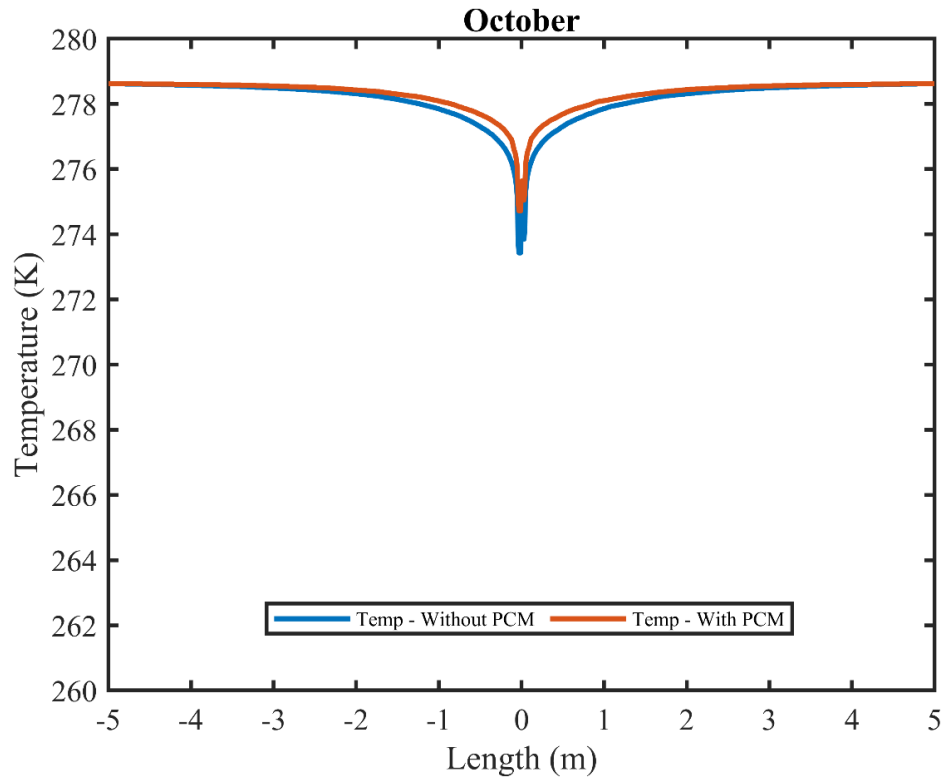
Figure 35: Ground temperature in October with and without PCM for a TAF with a normalized load of 0.4 tons (1406 W) in Duluth, MN

Figure 36 shows the temperature contour of the U-loop helical steel pile TAF in January for a small residential house in Duluth, MN, for a normalized load of 0.4 tons (1406 W), where (a) shows the temperature contour without PCM and (b) shows the temperature contour with PCM. It is visible that the temperature of the heat exchanger is around 273 K, or it is in the freezing temperature for both (a) without PCM and (b) with PCM. As January is in the winter season and the heating load is higher at that time, the outlet temperature of the heat exchanger drops below the freezing temperature. However, the soil temperature surrounding the pile is warmer than inside the pile as the ground is relatively warmer in winter than the ambient temperature. But the ground temperature in the vicinity of the pile is more warmer for the TAF with PCM in Figure 36 (b) than without PCM in Figure 36 (a), as the PCM stores heat in the ground, increasing the ground temperature.
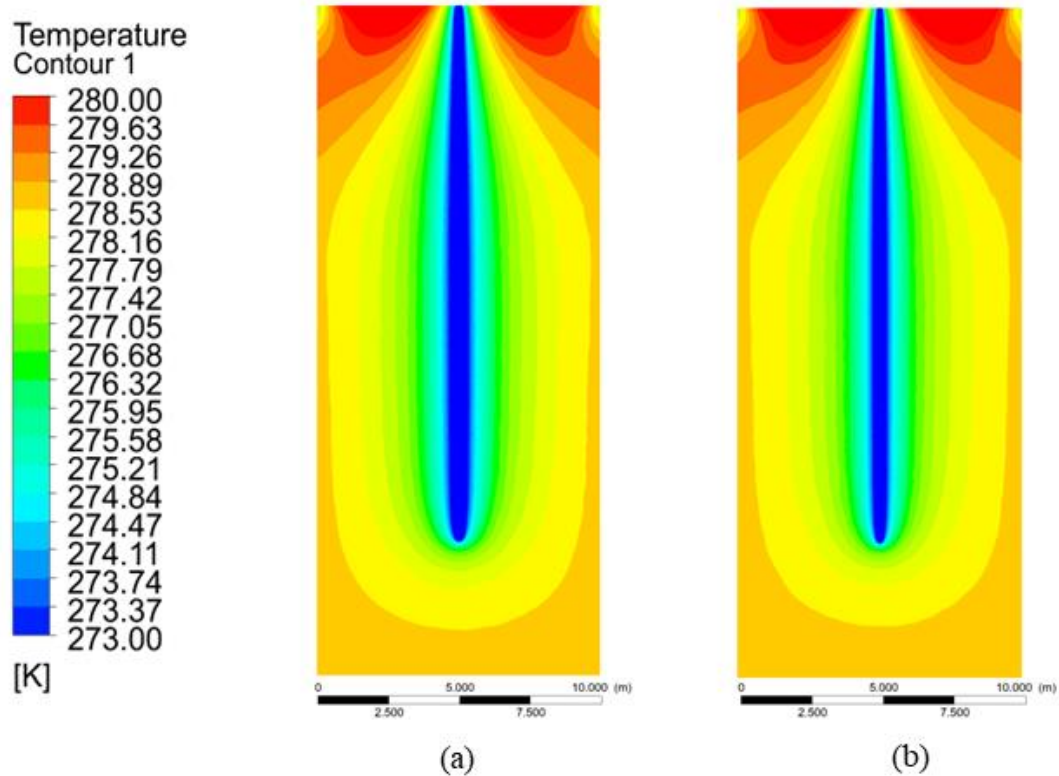
Figure 36: Temperature contour of U-loop helical steel pile TAF in January with a
normalized load of 0.4 tons (1406 W) in Duluth, MN (a) without PCM, (b) with PCM

Figure 37 shows the temperature contour of the U-loop helical steel pile TAF in July for a
small residential house in Duluth, MN, for a normalized load of 0.4 tons (1406 W), where
(a) shows the temperature contour without PCM and (b) shows the temperature contour
with PCM. It is visible that the temperature of the heat exchanger is above 273 K for both
(a) without PCM and (b) with PCM. As July is in the summer season and the cooling load
is higher at that time with no heating loads, the outlet temperature of the heat exchanger
goes above the freezing temperature. However, the pile's temperature is higher in Figure
37 (b) with PCM than in Figure 37 (a) without PCM, as the PCM stores heat in the ground,
which increases the ground temperature. As a result, the heat exchanger can discharge less
heat in the ground when using PCM, which makes the outlet temperature of the heat
exchanger higher than without PCM. Also, the soil temperature surrounding the pile using
PCM is slightly higher than without PCM for the same reason mentioned above. It is also

61

clearly visible that the temperatures of the pile and the ground changes with the seasonal changes over the year due to the variation of building loads and ambient temperature.
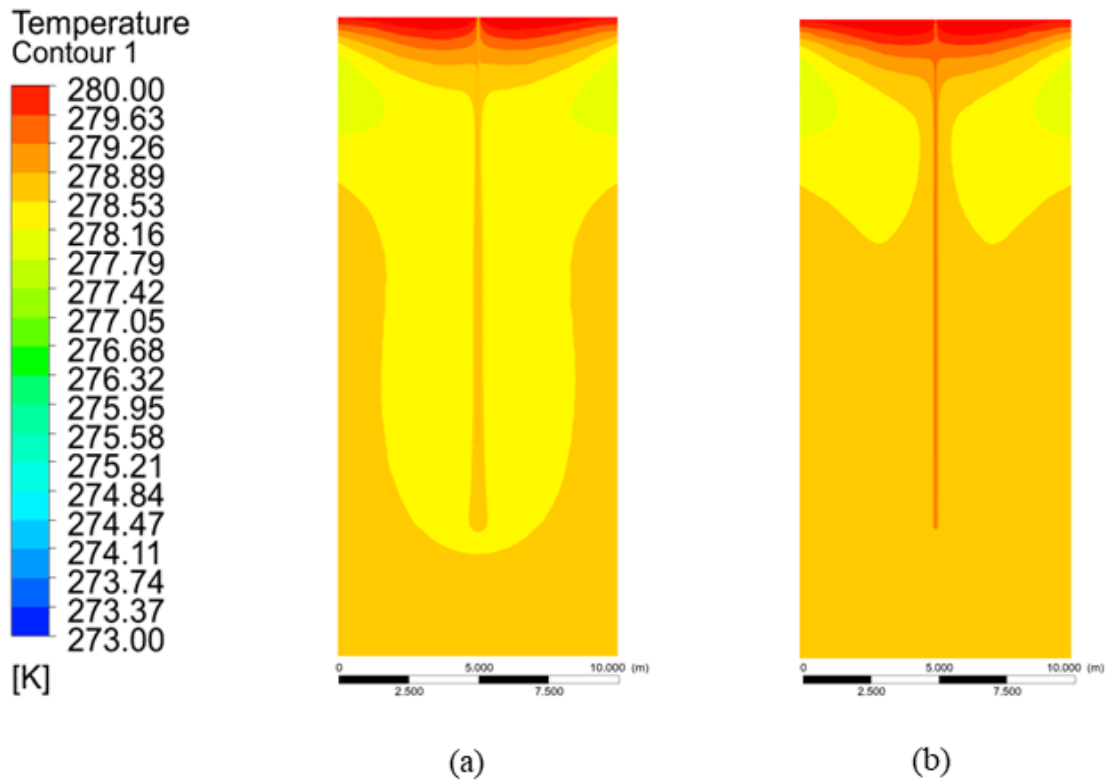
Figure 37: Temperature contour of U-loop helical steel pile TAF in July with a normalized load of 0.4 tons (1406 W) in Duluth, MN (a) without PCM, (b) with PCM

5.4 Thermal Performance of Pile TAF with PCM for Different Normalized Building Loads

As earlier discussed, PCM helps to enhance the performance of the heat pump over the year. Besides, an enhanced heat pump coupled with TAF needs less additional/auxiliary heating. To determine the capacity of each pile that gives a less amount or no amount of additional heating, different normalized building energy loads have been considered for Duluth, MN. The considered normalized building energy loads for each pile are 0.4 tons (1406 W), 0.33 tons (1160 W), and 0.25 tons (879 W). The cooling loads are the same for all these cases. Figure 38 shows the outlet temperature of the TAF with PCM for the considered normalized building loads. Based on a two-year analysis, the results show that

for 0.4 tons, there is a need for additional heating 5.8% of the year, for 0.33 tons additional heating is needed 5.6% of the year, and for 0.25 tons, additional heating is needed 1.12 % of the year. That means lowering the load helps to meet more building loads without additional heating.
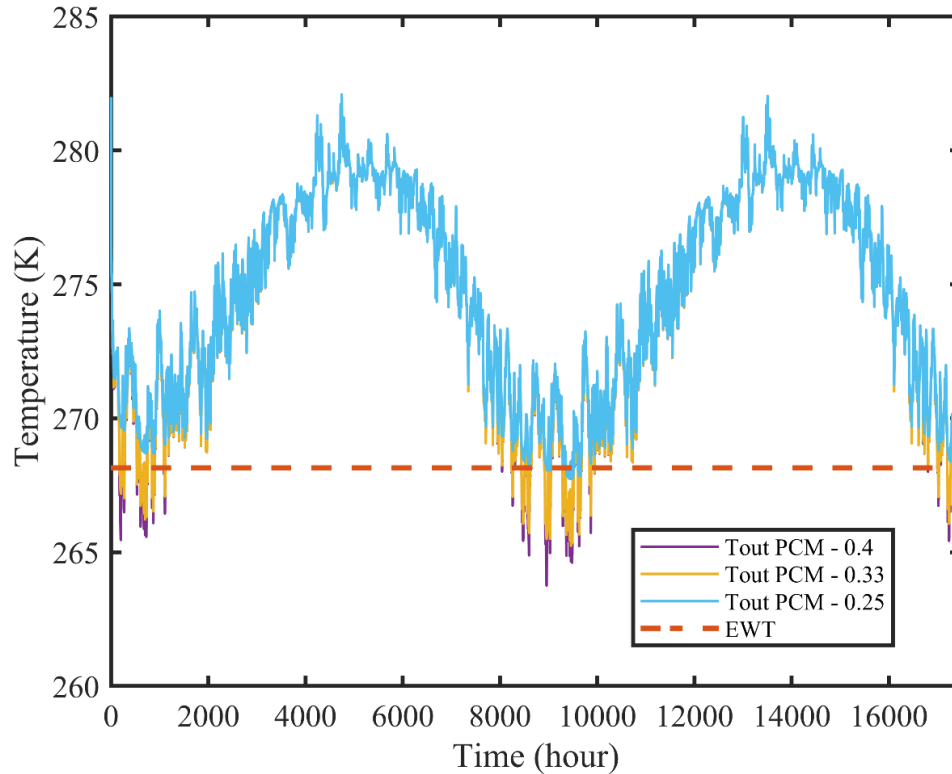
Figure 38: 2-year outlet temperature of TAF using PCM at 0.4, 0.33, and 0.25 tons load for Duluth, MN, and the minimum entering water temperature of the heat pump

From Figure 29 in section 5.2.1 for a five-year analysis, we have seen that, for a normalized building load of 0.4 tons, additional heating is required 6.30% of the year using PCM and that after the second year, the TAF outlet temperature does not change. But, if we want to meet the load of a typical small residential building considered in Duluth, MN, we have to meet around 3.28 tons of load in a year which needs a number of piles. Thus, if we use a normalized building load of 0.25 tons per pile, we will need 13 piles to meet all the loads with only 1.8% additional heating in a year for Duluth, MN. But, if we use 0.4 tons per pile, we will need only 8 piles to meet the entire home's energy loads with 5.8% additional heating requirements. Though the 0.25 tons load requires less additional heating, it will

cost more to install 13 piles than 8 piles for 0.4 tons of load for some extra additional heating. From the economic point of view, it is better to use 0.4 tons of load in a pile as it can save much more money that will be used for additional heating than 0.25 tons of load in a pile. So, for further analysis in different locations, 0.4 tons load is considered.

5.5 Loads at Different Locations in Minnesota

In this section, the building loads at different locations in Minnesota, such as Duluth, International Falls, and Saint Paul, have been analyzed and compared. Based on the calculations using BEopt [52] for a small house in Minnesota, the total annual heating energy consumptions for Duluth, International Falls, and Saint Paul are 82.58 MMBtu/yr, 110.65 MMBtu/yr, and 69.45 MMBtu/yr consecutively. The total annual cooling energy consumptions are 0.96 MMBtu/yr, 2.59 MMBtu/yr, and 3.42 MMBtu/yr. These calculations show that International Falls, MN has the highest heating energy demand in a year among these locations, and Saint Paul, MN has the highest cooling energy demand. Duluth, MN is a moderate climate among these three locations. That is why these locations were chosen to analyze the performance in a colder climate than Duluth, MN, and a warmer climate than Duluth, MN.

Figure 39 shows the normalized building energy load of 0.4 tons (1406 W) over one year for a typical small residential building with a basement in Duluth, MN. The positive loads are the cooling loads or loads during the summer, and the negative loads are the heating loads or loads during winter. Around 77.6% of the year, or around 283 days have heating loads. This means that the building needs heating 77.6% of the time in Duluth, MN. On the other hand, around 22.4% of the year, or around 82 days, there are cooling loads necessitating cooling during these days of the year. For the normalized load of 0.4 tons, the cooling load is 1.13% of the total annual load. Although heating is required only 77.6% of the year, the figure shows that about 98.86% of the building energy goes to providing heating.
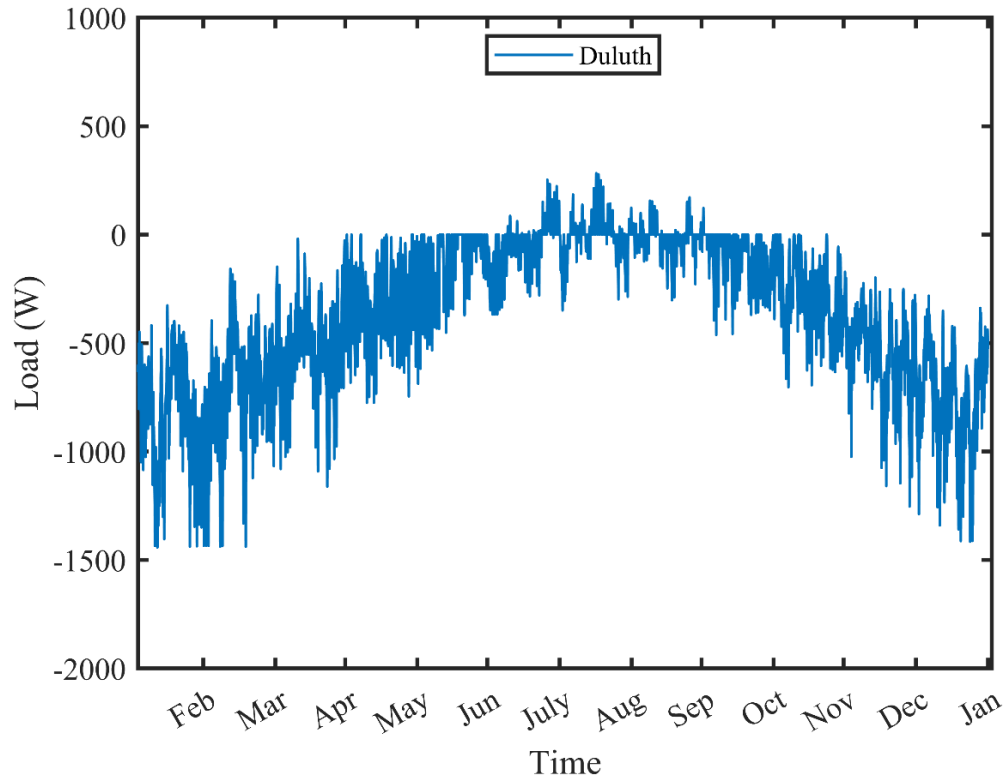
Figure 39: 0.4 tons (1406 W) of normalized load for Duluth, MN for a typical small residential building

Figure 40 shows the normalized building energy load of 0.4 tons (1406 W) over one year for a typical small residential building with a basement in International Falls, MN. Around 73.12% of the year, or around 267 days have heating loads. This means that the building needs heating 73.12% of the time in International Falls, MN. On the other hand, around 26.86% of the year, or around 98 days there are cooling loads necessitating cooling during these days of the year. For the normalized load of 0.4 tons, the cooling load is 1.72% of the total annual load. Although heating is required only 73.12% of the year, the figure shows that about 98.27% of the building energy goes to providing heating.

International Falls, MN needs heating for less number of days (16 days less) than Duluth MN, but the total annual heating energy needed is 28.07 MMBtu/yr more than Duluth. As the required heating energy demands significantly differ between Duluth and International Falls, this location is chosen to observe the system performance in a more colder place than Duluth in Minnesota.
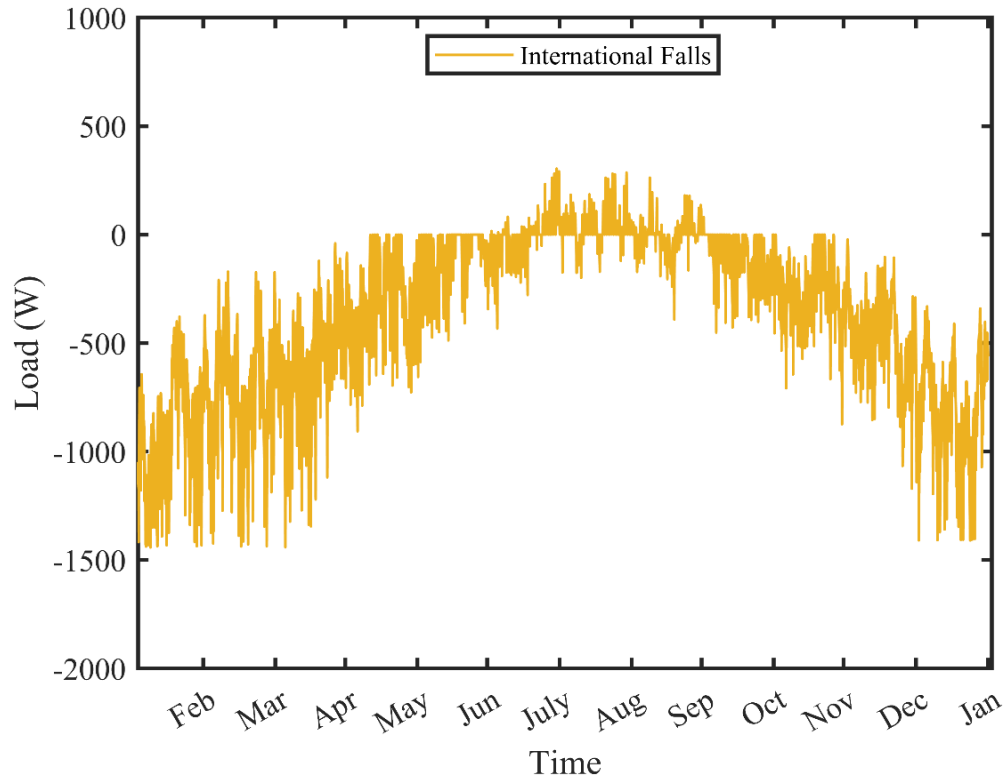
Figure 40: 0.4 tons (1406 W) of normalized load for International Falls, MN for a typical small residential building

Figure 41 shows the normalized building energy load of 0.4 tons (1406 W) over one year for a typical small residential building with a basement in Saint Paul, MN. Around 64.96% of the year, or around 237 days have heating loads. This means that the building needs heating 64.96% of the time in Saint Paul, MN. On the other hand, around 35% of the year, or around 128 days, there are cooling loads necessitating cooling during these days of the year. For the normalized load of 0.4 tons, the cooling load is 4.68% of the total annual load. Although heating is required only 64.96% of the year, the figure shows that about 95.31% of the building energy goes to providing heating.

Saint Paul, MN requires heating for a much less number of days (46 days less) than Duluth, MN, and cooling is required for more times of the year (46 days more) than Duluth, MN. As the cooling energy demands at Saint Paul are very high, around 2.46 MMBtu/yr more than Duluth, this location is chosen to observe the system performance in a more warmer place than Duluth in Minnesota.
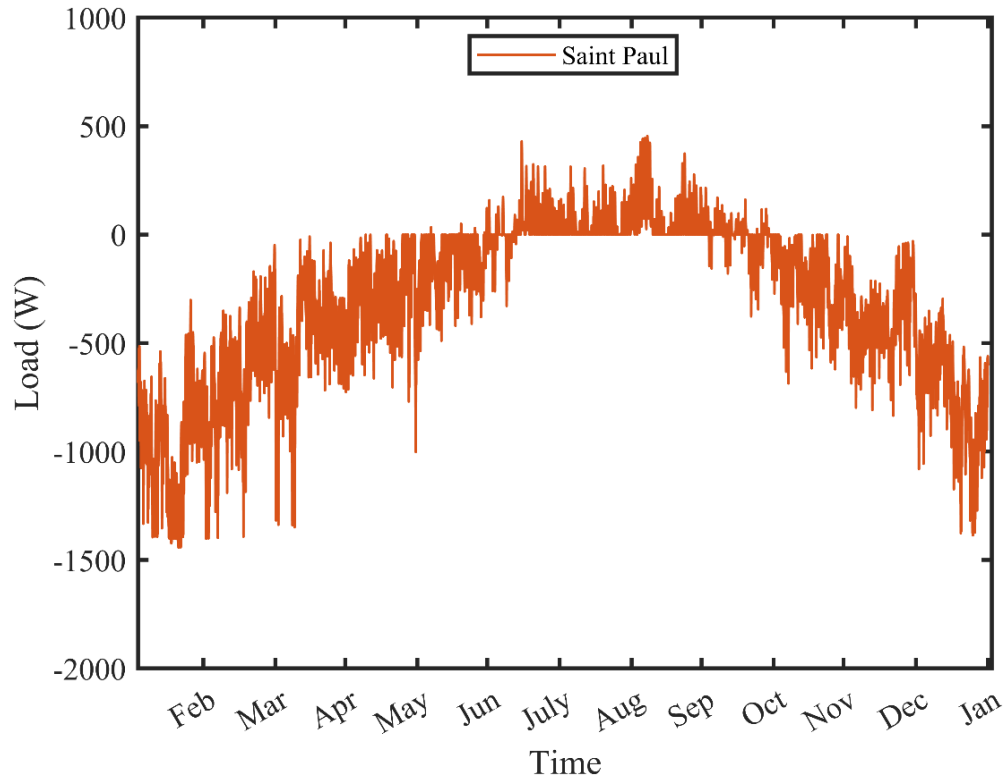
Figure 41: 0.4 tons (1406 W) of normalized load for Saint Paul, MN for a typical small residential building

5.6 Performance of Enhanced TAF at Different Locations

Figure 42 shows the outlet temperature of the TAF with and without PCM for two years for International Falls, MN for 0.4 tons of load. For the two years of operation, results show that the outlet temperature falls below the EWT 19.95% of the year without PCM and 12.23% of the year with PCM. This means that for 12.23% of the year, additional heating will be required for a typical small residential house in International Falls, MN which was 5.8% for Duluth, MN in a year for 0.4 tons of load using enhancement from PCM. This shows that having much higher heating energy demands in International Falls, MN reduces the performance than Duluth, MN, and requires more additional heating over the year.

67
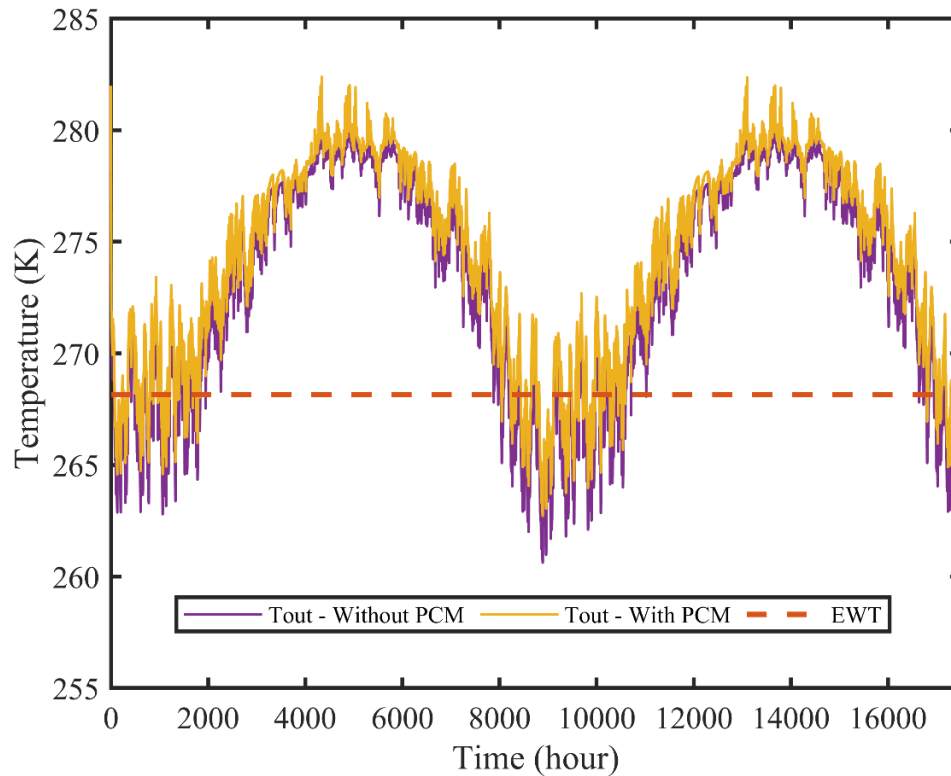
Figure 42: 2 years outlet temperature of the TAF with and without PCM vs entering water temperature of the heat pump for 0.4 tons (1406 W) of load for International Falls, MN

Figure 43 shows the outlet temperature of the TAF with and without PCM for two years for Saint Paul, MN for 0.4 tons of load. For the two years of operation, results show that the outlet temperature falls below the EWT 4.8% of the year without PCM and 2.23% of the year with PCM. This means that for 2.23% of the year, additional heating will be required for a typical small residential house in Saint Paul, MN which was 5.8% for Duluth in a year for 0.4 tons of load using enhancement from PCM. This shows that having much higher cooling energy demands and less heating energy demands in Saint Paul, MN increases the performance than Duluth, MN, and requires less additional heating over the year.
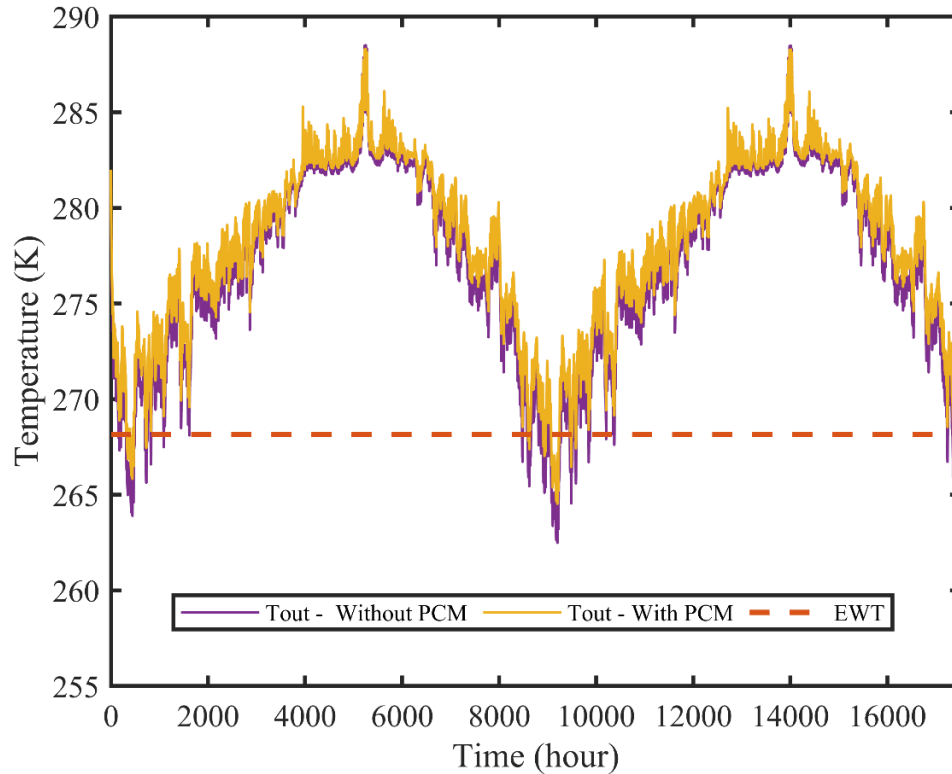
Figure 43: 2 years outlet temperature of the TAF with and without PCM vs entering water temperature of the heat pump for 0.4 tons (1406 W) of load for Saint Paul, MN

5.7 Heat Pump COP for Different Locations Using PCM

Figure 44 shows the heat pump COP for a helical pile TAF incorporating PCM for a normalized building energy load of 0.4 tons for Duluth, MN, International Falls, MN, and Saint Paul, MN. The average annual COP for all these locations with PCM is 4.09, 4.22, and 4.60, respectively. The average heating COP for these locations is 3.78, 3.74, and 3.90 with PCM. International Falls, MN, has the highest heating energy demand, making the heating COP lower than in other locations. Whereas Duluth, MN, has higher heating energy demands than Saint Paul, MN, and lower than International Falls, MN, which make the heating COP of Duluth, MN, slightly higher than International Falls, MN, but much lower than Saint Paul, MN.

On the other hand, the average cooling COP for these locations is 8.37, 8.34, and 7.49. Duluth, MN, has the lowest cooling energy demands, making the cooling COP higher for Duluth, MN, than other low locations. International Falls, MN, has higher cooling demand

69

than Duluth, MN, which makes the cooling COP slightly less than Duluth, MN. But Saint Paul, MN is the warmest place in all these locations and has the highest cooling demand, making the lowest cooling COP for Saint Paul, MN. But overall, the COP in Saint Paul, MN, is higher than in other places due to low heating demand throughout the year. This means that the helical pile TAFs work best for Saint Paul, MN, as it has the highest average COP and less additional heating requirements. On the other hand, International Falls, MN, has the worst performance as it requires more additional heating instead of having a higher COP than Duluth, MN. This means fewer piles will be needed for Saint Paul, MN than for International Falls, MN, making the implementation of the helical steel pile based TAFs cost-competitive.
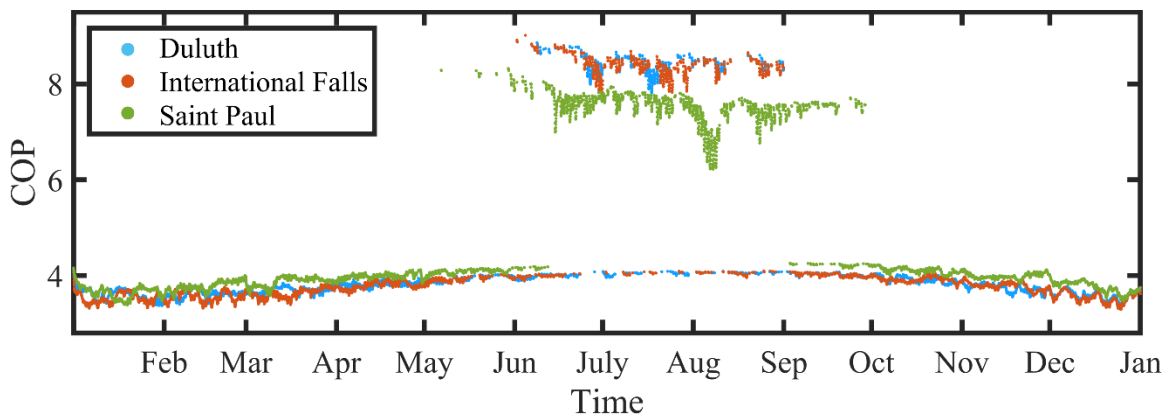
Figure 44: COP for Duluth, MN, International Falls, MN, and Saint Paul, MN for a normalized building energy load of 0.4 tons (1406 W) over a year using PCM

For a small residential house considered in this study, the load requirements for Duluth, MN, International Falls, MN, and Saint Paul, MN are around 3.28 tons, 3.43 tons, and 3.11 tons respectively. Considering 0.4 tons per pile, the number of piles required for each of these locations are 8, 9, and 8. So, it also shows that the system performs best in Saint Paul, MN owing to lower loads, and worst in International Falls, MN owing to higher loads which also increases the required number of piles causing more capital cost.

Chapter 6 - Conclusions

This study numerically considered the transient short-term (one year) and long-term (five-year) performance of a helical steel pile thermo-active foundation coupled with a ground-source heat pump. A thoroughly validated and verified numerical model, coupled with actual building energy loads and climatic conditions, was used to investigate the influence of different flow rates and pile locations under the building foundation on the system's performance. Additionally, the effect of latent thermal energy storage using phase change materials (PCM) as an enhancement on the system's performance has also been investigated for different normalized building energy loads and locations in Minnesota (Duluth, International Falls, and Saint Paul).

To analyze the effect of different laminar flow velocities (0.12 m/s (1 gpm), 0.2 m/s (1.67 gpm), 0.25 m/s (2.08 gpm), and 0.3 m/s (2.54 gpm)) and different turbulent velocities (0.8 m/s (6.65 gpm), 1.6 m/s (13.3 gpm), 2.4 m/s (19.95 gpm), and 3.2 m/s (26.6 gpm)), the results show that the coefficient of performance (COP) does not vary significantly with increasing flow rates, remaining around 3.3, but the deltaT (temperature difference) decreases gradually. On the other hand, the pump power increases with higher flow rates, making the laminar flow rates a better choice for the system's operation as they ensure a comparable performance while consuming less pump power. Moreover, the study of different pile locations under the building footprint for Duluth, with a 0.4 tons (1406 W) load, showed that the overall performance of the system does not change with the pile locations, but there are some seasonal variations in the COP. As a result, the pile can be located anywhere under the building.

To analyze the long-term performance of a thermo-active foundation enhanced with PCM, two PCM tubes of 0.0053093 m^3 (5.30 kg) volume each were embedded outside the foundation close to the U-tube heat exchanger. The results show that, for a normalized building energy load of 0.4 tons (1406 W) for a typical small residential building in Duluth, MN, the system meets the building load 85.42% of the year without any enhancement and 92.70% with PCM. Therefore, PCM helps meet the building loads per pile by 8.28% more annually. To further explore the performance with different loads, 0.33 tons (1160 W) and

71

0.25 tons (879 W) of normalized building energy loads were investigated for Duluth, MN. Considering long-term performance, the results show that for 0.33 tons, the heat pump will not work for 5.6% of the year, and for 0.25 tons of load, the heat pump will not work for 1.12% of the year. As a result, additional heating source will be required during these times of the year per pile to meet the total building load.

Using a normalized building energy load of 0.25 tons per pile will require 13 piles to meet the total building load of 3.28 tons in a year while using 0.4 tons per pile will only require 8 piles to meet the load with 5.8% additional heating in a year, which is more economical than using 13 piles. Moreover, the annual average COP using PCM is around 4.09, compared to 4.04 without PCM, for a normalized building energy load of 0.4 tons for a typical small residential building in Duluth, MN, ensuring an overall enhancement of the performance of the TAF using PCM.

To analyze the system's performance in colder and warmer environments than Duluth, MN, the TAF using PCM was explored in International Falls, MN, and Saint Paul, MN. Due to the highest heating energy demand among these locations, International Falls requires auxiliary heating for 12.23% of the year with a normalized building energy load of 0.4 tons per pile. On the other hand, Saint Paul requires only 2.23% additional heating for 0.4 tons per pile, as it has the highest cooling energy demand and the lowest heating energy demand among these locations. Moreover, the COP for Duluth, International Falls, and Saint Paul using PCM and a normalized building energy load of 0.4 tons (1406 W) is around 4.09, 4.22, and 4.60, respectively. This means that the system works best for Saint Paul, MN, moderately for Duluth, MN, and has the lowest performance for International Falls, MN, despite having a slightly higher overall COP than Duluth, MN.

Chapter 7 - Future Research and Recommendations

The study of GSHP and TAF required long-term hourly studies to characterize their performance accurately. In this work, studies have considered long-term and short-term performance for three locations in Minnesota for a helical steel TAF using a U-loop heat exchanger. Owing to the variety of configurations, and operating conditions, additional studies are recommended for a full understanding of the TAF in different climatic conditions and cost competitiveness for long-term operation. The future recommendations of this study are listed below-

- In this study, one configuration of the U-loop heat exchanger for the helical pile based TAF is used, given the long-term nature of the simulations and considerations of different locations. As such, different geometries of TAFs should be considered in the future to determine any performance improvements.
- The soil thermal conductivity for different locations should be explored from detailed soil tests or thermal response tests for better accuracy.
- This study has been done for representative locations i.e., Duluth, MN, International Falls, MN, and Saint Paul, MN. Other locations in Minnesota and throughout the US should also be explored to understand performance in diverse climate conditions.
- In this study, two PCM tubes placed in the ground around the steel pile have been used to investigate the effect of thermal energy storage and performance enhancement. It is recommended that more PCM tubes and different locations of the PCM tubes around or inside the pile be considered to explore the potential benefits. Moreover, other means of integrating PCM, such as mixing the PCM with the backfill material, and using microencapsulated PCMs, among others should be considered.

References

[1]   B. Nordell, "Thermal pollution causes global warming," *Glob. Planet. Change*, vol. 38, no. 3–4, pp. 305–312, 2003, doi: 10.1016/S0921-8181(03)00113-9.

[2]   T. Inflation and R. Act, "WHAT HAS THE U . S . DONE," pp. 19–20, 2022.

[3]   E. and I. E. A. UN, *Towards a zero-emission, efficient, and resilient buildings and construction sector*. 2017. [Online]. Available: www.globalabc.org

[4]   "IEA (2022), Buildings, IEA, Paris https://www.iea.org/reports/buildings, License: CC BY 4.0".

[5]   L. Pérez-Lombard, J. Ortiz, and C. Pout, "A review on buildings energy consumption information," *Energy Build.*, vol. 40, no. 3, pp. 394–398, 2008, doi: 10.1016/j.enbuild.2007.03.007.

[6]   C. Robinson *et al.*, "Machine learning approaches for estimating commercial building energy consumption," *Appl. Energy*, vol. 208, no. September, pp. 889–904, 2017, doi: 10.1016/j.apenergy.2017.09.060.

[7]   A. Mustafa Omer, "Ground-source heat pumps systems and applications," *Renewable and Sustainable Energy Reviews*, vol. 12, no. 2. pp. 344–371, Feb. 2008. doi: 10.1016/j.rser.2006.10.003.

[8]   "5 Things You Should Know about Geothermal Heat Pumps, Office of Energy Efficiency and Renewable Energy, US Department of Energy.", [Online]. Available: https://www.energy.gov/eere/articles/5-things-you-should-know-about-geothermal-heat-pumps

[9]   A. K. Sani, R. M. Singh, T. Amis, and I. Cavarretta, "A review on the performance of geothermal energy pile foundation, its design process and applications," *Renew. Sustain. Energy Rev.*, vol. 106, no. February, pp. 54–78, 2019, doi: 10.1016/j.rser.2019.02.008.

[10]   P. Christodoulides, L. Aresti, and G. Florides, "Air-conditioning of a typical house in moderate climates with Ground Source Heat Pumps and cost comparison with Air Source Heat Pumps," *Appl. Therm. Eng.*, vol. 158, no. May, p. 113772, 2019, doi: 10.1016/j.applthermaleng.2019.113772.

[11]   Y. L. E. Law and S. B. Dworkin, "Characterization of the effects of borehole configuration and interference with long term ground temperature modelling of ground source heat pumps," *Appl. Energy*, vol. 179, pp. 1032–1047, 2016, doi: 10.1016/j.apenergy.2016.07.048.

[12]   N. Zhu, P. Hu, L. Xu, Z. Jiang, and F. Lei, "Recent research and applications of ground source heat pump integrated with thermal energy storage systems: A review," *Appl. Therm. Eng.*, vol. 71, no. 1, pp. 142–151, 2014, doi: 10.1016/j.applthermaleng.2014.06.040.

[13]   Q. Gao, M. Li, M. Yu, J. D. Spitler, and Y. Y. Yan, "Review of development from GSHP to UTES in China and other countries," *Renew. Sustain. Energy Rev.*, vol. 13, no. 6–7, pp. 1383–1394, 2009, doi: 10.1016/j.rser.2008.09.012.

[14]   H. Brandl, "Energy foundations and other thermo-active ground structures," *Geotechnique*, vol. 56, no. 2, pp. 81–122, 2006, doi: 10.1680/geot.2006.56.2.81.

[15]   R. M. Singh, A. K. Sani, and T. Amis, *An overview of ground-source heat pump technology*. Elsevier Inc., 2018. doi: 10.1016/B978-0-12-814104-5.00015-6.

[16]   Q. Lu, G. A. Narsilio, G. R. Aditya, and I. W. Johnston, "Economic analysis of

vertical ground source heat pump systems in Melbourne," *Energy*, vol. 125, pp. 107–117, 2017, doi: 10.1016/j.energy.2017.02.082.

[17] S. J. Self, B. V. Reddy, and M. A. Rosen, "Geothermal heat pump systems: Status review and comparison with other heating options," *Appl. Energy*, vol. 101, pp. 341–348, 2013, doi: 10.1016/j.apenergy.2012.01.048.

[18] A. Michopoulos, T. Zachariadis, and N. Kyriakis, "Operation characteristics and experience of a ground source heat pump system with a vertical ground heat exchanger," *Energy*, vol. 51, pp. 349–357, 2013, doi: 10.1016/j.energy.2012.11.042.

[19] H. Javadi, S. S. Mousavi Ajarostaghi, M. A. Rosen, and M. Pourfallah, "Performance of ground heat exchangers: A comprehensive review of recent advances," *Energy*, vol. 178. pp. 207–233, 2019. doi: 10.1016/j.energy.2019.04.094.

[20] M. A. Rosen and S. Koohi-Fayegh, *Geothermal energy: sustainable heating and cooling using the ground*. John Wiley & Sons, 2017.

[21] I. Sarbu and C. Sebarchievici, "General review of ground-source heat pump systems for heating and cooling of buildings," *Energy Build.*, vol. 70, pp. 441–454, 2014, doi: 10.1016/j.enbuild.2013.11.068.

[22] Z. Liu, W. Xu, C. Qian, X. Chen, and G. Jin, "Investigation on the feasibility and performance of ground source heat pump (GSHP) in three cities in cold climate zone, China," *Renew. Energy*, vol. 84, pp. 89–96, Dec. 2015, doi: 10.1016/j.renene.2015.06.019.

[23] K. Bakirci, "Evaluation of the performance of a ground-source heat-pump system with series GHE (ground heat exchanger) in the cold climate region," *Energy*, vol. 35, no. 7, pp. 3088–3096, 2010, doi: 10.1016/j.energy.2010.03.054.

[24] N. Naili, M. Hazami, I. Attar, and A. Farhat, "In-field performance analysis of ground source cooling system with horizontal ground heat exchanger in Tunisia," *Energy*, vol. 61, pp. 319–331, 2013, doi: 10.1016/j.energy.2013.08.054.

[25] Z. Mohamad, F. Fardoun, and F. Meftah, "A review on energy piles design, evaluation, and optimization," *J. Clean. Prod.*, vol. 292, p. 125802, 2021, doi: 10.1016/j.jclepro.2021.125802.

[26] Y. Hamada, H. Saitoh, M. Nakamura, H. Kubota, and K. Ochifuji, "Field performance of an energy pile system for space heating," *Energy Build.*, vol. 39, no. 5, pp. 517–524, 2007, doi: 10.1016/j.enbuild.2006.09.006.

[27] J. Fadejev, R. Simson, J. Kurnitski, and F. Haghighat, "A review on energy piles design, sizing and modelling," *Energy*, vol. 122, pp. 390–407, 2017, doi: 10.1016/j.energy.2017.01.097.

[28] S. R. Nicholson, L. R. Kober, P. Atefrad, A. Mwesigye, and S. B. Dworkin, "The influence of geometry on the performance of a helical steel pile as a geo-exchange system," *Renew. Energy*, vol. 172, pp. 714–727, 2021, doi: 10.1016/j.renene.2021.03.067.

[29] Jalaluddin, A. Miyara, K. Tsubaki, S. Inoue, and K. Yoshida, "Experimental study of several types of ground heat exchanger using a steel pile foundation," *Renew. Energy*, vol. 36, no. 2, pp. 764–771, 2011, doi: 10.1016/j.renene.2010.08.011.

[30] D. Wu, H. Liu, G. Kong, and C. Li, "Thermo-mechanical behavior of energy pile under different climatic conditions," *Acta Geotech.*, vol. 14, no. 5, pp. 1495–1508, 2019, doi: 10.1007/s11440-018-0731-9.

[31] A. Darbandi, S. Davani, J. Gruenes, P. Agarwala, A. Hoxie, and A. Mwesigye, "Long-Term Thermal Performance Analysis of a Horizontal Foundation Heat Exchanger for Space Heating and Cooling in Extremely Cold Climates," pp. 1747–1757, 2023, doi: 10.1615/tfec2023.rfs.045922.

[32] S. Davani, A. Darbandi, P. Agarwala, J. Gruenes, A. Hoxie, and A. Mwesigye, "Design and Performance Analisys of Slinkytm Type Foundation Heat Exchangers for Space Heating and Cooling in a Cold Climate," pp. 569–578, 2023, doi: 10.1615/tfec2023.ens.046078.

[33] P. Agarwala, S. Davani, A. Darbandi, J. Gruenes, A. Hoxie, and A. Mwesigye, "Thermal Performance Analysis of Helical Steel Thermo-Active Foundations for Cold Climates," *ASHRAE SCANVAC HVAC Cold Clim. Conf.*, 2023, [Online]. Available: https://www.techstreet.com/ashrae/standards/thermal-performance-analysis-of-helical-steel-thermo-active-foundations-for-cold-climates?product_id=2564739

[34] Rubitherm, "Techdata_-RT2HC_EN_30092020," p. 2020, 2020, [Online]. Available: https://www.rubitherm.eu/media/products/datasheets/Techdata_-RT2HC_EN_30092020.PDF

[35] M. M. Farid, A. M. Khudhair, S. A. K. Razack, and S. Al-Hallaj, "A review on phase change energy storage: Materials and applications," *Energy Convers. Manag.*, vol. 45, no. 9–10, pp. 1597–1615, 2004, doi: 10.1016/j.enconman.2003.09.015.

[36] T. Cooling, J. Skovajsa, M. Koláˇ, and M. Zálešák, "Phase Change Material Based Accumulation Panels in," 2017, doi: 10.3390/en10020152.

[37] R. Baetens, B. P. Jelle, and A. Gustavsen, "Phase change materials for building applications: A state-of-the-art review," *Energy Build.*, vol. 42, no. 9, pp. 1361–1368, 2010, doi: 10.1016/j.enbuild.2010.03.026.

[38] F. Ishola, P. Babalola, O. Olatunji, I. Ogunrinola, O. Ayo, and S. Akinlabi, "Succinct Review on State-of-art Carbon-based Phase Change Material for Solar Thermal Storage Applications," *E3S Web Conf.*, vol. 152, pp. 3–6, 2020, doi: 10.1051/e3sconf/202015202008.

[39] M. Bottarelli, M. Bortoloni, Y. Su, C. Yousif, A. A. Aydın, and A. Georgiev, "Numerical analysis of a novel ground heat exchanger coupled with phase change materials," *Appl. Therm. Eng.*, vol. 88, pp. 369–375, 2015, doi: 10.1016/j.applthermaleng.2014.10.016.

[40] Y. Lyne, H. Paksoy, and M. Farid, "Laboratory investigation on the use of thermally enhanced phase change material to improve the performance of borehole heat exchangers for ground source heat pumps," *Int. J. Energy Res.*, vol. 43, no. 9, pp. 4148–4156, 2019, doi: 10.1002/er.4522.

[41] M. Kong, J. L. Alvarado, C. Thies, S. Morefield, and C. P. Marsh, "Field evaluation of microencapsulated phase change material slurry in ground source heat pump systems," *Energy*, vol. 122, pp. 691–700, 2017, doi: 10.1016/j.energy.2016.12.092.

[42] P. McKenna, W. J. N. Turner, and D. P. Finn, "Geocooling with integrated PCM thermal energy storage in a commercial building," *Energy*, vol. 144, pp. 865–876, 2018, doi: 10.1016/j.energy.2017.12.029.

[43] X. Li, C. Tong, L. Duanmu, and L. Liu, "Research on U-tube Heat Exchanger with Shape-stabilized Phase Change Backfill Material," *Procedia Eng.*, vol. 146, pp. 640–647, 2016, doi: 10.1016/j.proeng.2016.06.420.

[44]   F. Chen, J. Mao, S. Chen, C. Li, P. Hou, and L. Liao, "Efficiency analysis of utilizing phase change materials as grout for a vertical U-tube heat exchanger coupled ground source heat pump system," *Appl. Therm. Eng.*, vol. 130, pp. 698–709, 2018, doi: 10.1016/j.applthermaleng.2017.11.062.

[45]   A. Alkhwildi, R. Elhashmi, and A. Chiasson, "Parametric modeling and simulation of Low temperature energy storage for cold-climate multi-family residences using a geothermal heat pump system with integrated phase change material storage tank," *Geothermics*, vol. 86, no. May, p. 101864, 2020, doi: 10.1016/j.geothermics.2020.101864.

[46]   M. Alavy, M. Peiris, J. Wang, and M. A. Rosen, "Assessment of a novel phase change material-based thermal caisson for geothermal heating and cooling," *Energy Convers. Manag.*, vol. 234, no. November 2020, p. 113928, 2021, doi: 10.1016/j.enconman.2021.113928.

[47]   S. Shukla, A. M. Bayomy, S. Antoun, A. Mwesigye, W. H. Leong, and S. B. Dworkin, "Performance characterization of novel caisson-based thermal storage for ground source heat pumps," *Renew. Energy*, vol. 174, pp. 43–54, 2021, doi: 10.1016/j.renene.2021.04.075.

[48]   M. M. Mousa, A. M. Bayomy, and M. Z. Saghir, "Long-term performance investigation of a GSHP with actual size energy pile with PCM," *Appl. Therm. Eng.*, vol. 210, no. March, p. 118381, 2022, doi: 10.1016/j.applthermaleng.2022.118381.

[49]   P. Huelman, T. Schirber, G. Mosiman, R. Jacobson, T. M. Smith, and M. Li, "Residential ground source heat pump study: a comprehensive assessment of performance, emissions, and economics," *Minnesota Conserv. Appl. Res. Dev. Final Rep.*, 2016.

[50]   A. Fluent, "ANSYS fluent theory guide 15.0," *ANSYS, Canonsburg, PA*, vol. 33, 2013.

[51]   A. Fluent, "12.0 User's guide," *Ansys inc*, vol. 6, p. 552, 2009.

[52]   C. Christensen, R. Anderson, S. Horowitz, A. Courtney, and J. Spencer, "Energy Efficiency and Renewable Energy Building Technologies Program T OF E N BEopt™ Software for Building Energy Optimization: Features and Capabilities," no. August, 2006, [Online]. Available: http://www.osti.gov/bridge

[53]   C. Li, J. Mao, H. Zhang, Z. Xing, Y. Li, and J. Zhou, "Numerical simulation of horizontal spiral-coil ground source heat pump system: Sensitivity analysis and operation characteristics," *Appl. Therm. Eng.*, vol. 110, pp. 424–435, 2017, doi: 10.1016/j.applthermaleng.2016.08.134.

[54]   A. Geothermal and H. Pump, "Engineering Specification Liquid to Air Geothermal Heat Pump," vol. 4, no. 506, 2022.

[55]   L. U. Xing, "Estimations of Undisturbed Ground Temperatures using Numerical and Analytical Modeling," 2010.

[56]   Dynalene Inc., "Dynalene Propylene Glycol Series," vol. 9686, no. 610, 2008, [Online]. Available: https://www.dynalene.com/wp-content/uploads/2020/05/Dynalene-PG-Tech-Data-Sheet-Rev1.pdf

[57]   G. A. Longo, S. Mancin, G. Righetti, and C. Zilio, "Experimental measurement of thermophysical properties of some commercial phase change materials (PCM) for air conditioning applications," *Int. J. Refrig.*, vol. 144, no. July, pp. 202–210, 2022, doi: 10.1016/j.ijrefrig.2022.08.007.

[58] "Weather Data by Country", [Online]. Available: https://energyplus.net/weather-region/north_and_central_america_wmo_region_4/USA/MN

[59] U. of Minnesota, "Minnesota Geological Survey", [Online]. Available: https://conservancy.umn.edu/handle/11299/57196

[60] U. S. D. of Agriculture, "Web Soil Survey", [Online]. Available: https://websoilsurvey.nrcs.usda.gov/app/WebSoilSurvey.aspx

[61] G. Dalla Santa *et al.*, "An updated ground thermal properties database for GSHP applications," *Geothermics*, vol. 85, p. 101758, 2020.

[62] J. M. Andújar Márquez, M. Á. Martínez Bohórquez, and S. Gómez Melgar, "Ground thermal diffusivity calculation by direct soil temperature measurement. Application to very low enthalpy geothermal energy systems," *Sensors*, vol. 16, no. 3, p. 306, 2016.

[63] L. Laloui, R. Loria, and A. F. Chapter, "Heat and mass transfers in the context of energy geostructures," *Anal. Des. Energy Geostructures*, pp. 69–135, 2020.

[64] M. Sakry, "Geothermal Parameters," *Insects Close Up*, pp. 81–81, 2021, doi: 10.1525/9780520349711-054.

[65] Jalaluddin and A. Miyara, "Thermal performance investigation of several types of vertical ground heat exchangers with different operation mode," *Appl. Therm. Eng.*, vol. 33–34, no. 1, pp. 167–174, 2012, doi: 10.1016/j.applthermaleng.2011.09.030.